

# A 3-d simulation of the atmospheric neutrinos

J.Favier <sup>\*1</sup>, R.Kossakowski and J.P Vialle

Laboratoire d'Annecy-le-Vieux de Physique des Particules, LAPP,  
IN2P3-CNRS, BP 110, F-74941 Annecy-le-Vieux, CEDEX, France

## Abstract

The first AMS flight in June 1998 on board of the space shuttle Discovery at an altitude of approximately 380 km unveiled unexpected features of the cosmic rays spectra below the Earth geomagnetic cut-off. In addition to a secondary flux of particles at all latitude, a ring of high energy particles (up to 6 GeV) and an anomalous ratio  $e^+/e^-$  as high as 4 was observed near the geomagnetic equator. This paper describes a simulation of the interaction of primary cosmic rays with atmosphere in which the effect of the Earth magnetic field is included. Using the GEANT3 package for the tracking of particles with the GFLUKA associated package for the physics of interactions, this simulation reproduces quite well the AMS experimental results and the CAPRICE muon data at ground level. The predictions of this model for the flux of atmospheric neutrino are compared with the Super-Kamiokande results and with the results of other atmospheric neutrino models.

---

<sup>1\*</sup>Corresponding author; e-mail: Jean.Favier@lapp.in2p3.fr

# 1 Introduction

The Super-Kamiokande data on atmospheric neutrinos which show a strong evidence for  $\nu_\mu - \nu_\tau$  oscillations has stressed the need for accurate calculation of atmospheric neutrino fluxes and production mechanisms. After pioneering simulation works [1, 2, 3], it became obvious that the Earth magnetic field has an important effect on the flux of primary and secondary cosmic rays [4, 5, 6], , which leads to the need of full 3D simulation. Meanwhile, from the measurements of cosmic ray fluxes by the AMS[7, 8, 9, 10, 11], BESS[13], and CAPRICE[12] experiments, new inputs to the generators had become available, and new experimental data were also available allowing to check how accurately a model could predict fluxes. This comprises the measurement of cosmic muon yields at different latitudes and altitudes by CAPRICE, and since AMS precursor flight on board of the space shuttle Discovery in 1998, the secondary proton and electron fluxes coming from the interaction of primary cosmic rays (mainly protons and alphas) with the Earth atmosphere [7]-[11].

Below are presented the results of a full 3D simulation based on the GEANT3.2.1 package, which was used in most of the high energy physics experiments and was extensively tested in various conditions. In this simulation, primary protons, alphas, positrons and electrons from outer space in the energy range 0.2 to 500 GeV are traced through the Earth magnetic field. A part of them impinge on the atmosphere and interact, producing secondary hadrons and leptons. These fluxes and yields are compared with experimental data. Neutrino distribution predictions are calculated at the geographic location of the Super-Kamiokande experiment and compared with the results of other models. The predictions on absolute fluxes are all normalised from only one parameter, namely the yield of 100 GeV primary cosmic rays measured by AMS[11].

This work was started in 1999 to understand the unexpected features of charged cosmic ray fluxes measured by AMS. First results were presented to the AMS collaboration in November 1999 reproducing pretty well the AMS data though using only a simple dipole to model the Earth magnetic field[14].

## 2 Simulation scheme

### 2.1 Primary generation

It is generally admitted that far from Earth, charged cosmic rays density is homogeneous and isotropically distributed in direction, while the rigidity distribution is well represented by a power law with a negative exponent close to 2.7. The Earth magnetic field induces a distortion of this spectrum at rigidity below 30 GV with eventually a rigidity cut-off which varies with the geomagnetic latitude. For instance to reach the Earth surface at the geomagnetic equator, protons must have a kinetic energy greater than 10 GeV.

To reproduce by simulation these fluxes without biases, several methods were tried. The most straightforward way (so-called method B below), which relies only on the properties of cosmic ray distribution mentioned above, is to generate particles isotropically on an external sphere of radius  $R_{ex}$  large enough to be beyond the Earth's magnetosphere and to trace the particles down to the Earth. Unfortunately, such a method is heavily consuming computer time since many particles do not reach the Earth vicinity even if they are inside a momentum dependent pre-calculated angular cone ( fig.1). In the most commonly used method (so-called method A below), it is advocated that due to Liouville's theorem, particles can be generated isotropically near the Earth's surface, despite the spatial dis-

tortion induced by the Earth magnetic field on momentum and space densities. To take it into account, particles generated isotropically near the Earth's surface are charge-inverted and traced back in the magnetic field, and only those trajectories which reach the surface of the external sphere  $R_{ex}$  are kept and then traced forward to Earth, this time taking into account interaction processes in the atmosphere. Such a method obviously allows to minimize computing time, its efficiency being only governed by the cut-off effect.

When the Earth magnetic field and the absorbing Earth are taken into account, the validity of method A could be questioned. Thus, before using method A, we have made a very high statistic simulation with both A and B methods. The distribution obtained for key variables were found to be identical (fig.2) , which allowed us to use method A for the rest of the study. It was found that to avoid distortion in the spectra, the radius  $R_{ex}$  of the external sphere has to be as high as 20 Earth radius ( while most of the authors are using  $R_{ex} = 10$  Earth radius for both method A and B, which overestimates by about 5% the flux of particle at low energy, as seen on fig.3).

For the simulation, the Earth is represented by a sphere of radius  $R_0 = 6371.2$  km. The Earth atmosphere is modeled as 82 concentric spherical layers, with a thickness of 1 km for the 50 first ones and 2 km for the remaining 32 (fig.4). The air density in each layer is calculated according to the NASA standard model [15] of atmosphere. As a matter of fact, the density of the upper layer is as low as  $0.103 \cdot 10^{-7} \text{ gr/cm}^3$ . The standard IGRF field[17] representation with Legendre polynomials up to  $10^{th}$  order is used for the Earth magnetic field, with coefficients corresponding to the date of the AMS01 flight (June 1998). A factor of 30 in tracking computing time was saved by interpolating this field from a pre-calculated 3D field map grid rather than calculating the field at each tracking step. We checked that the residuals of these interpolations are below 0.5%. The Sun effect on the field is neglected. Particles are generated following method A from a spherical layer at 380 km in altitude, with a radius of the external sphere  $R_{ex} = 20 R_0$

The primary particle spectra (p,  $\alpha$ , e+, e-) are taken from the measurements published by the AMS collaboration[10], compatible with a power law rigidity spectrum of  $T^{-2.78}$  at high energy, and the solar modulation is included as a rigidity-dependent weight[16]. To minimize statistical uncertainties at the generation level, the primaries are generated flat in six energy slices ( in GeV: 0.2-0.5, 0.5-2., 2.-6., 6.-30., 30.-200., 200.-500.), and the events are weighted during the analysis according to the AMS primary fluxes distributions. Other components of cosmic rays have been neglected. The accepted primary cosmic rays representing more than a milion tracks have been recorded on files and used as input for the simulations of cascades in the atmosphere.

## 2.2 Interaction with atmosphere and detection of particles

The secondary particle fluxes are quite sensitive to the quality of the description of hadronic interactions. The standard GEISHA hadronic package of GEANT 3 was found being less accurate than the GFLUKA package when comparing the predicted secondary particles fluxes to the AMS measured ones for electrons, positrons and protons. We thus used only GFLUKA for the results shown below. Neutrinos energy spectra predicted using GFLUKA are also found closer to the prediction of other models not making use of GEANT 3 for simulation; the ratio of fluxes obtained with GFLUKA and GEISHA as a function of neutrino energy is shown in fig.5 and reveals deviations up to 30%.

Tracking in the geomagnetic field is stopped when the kinetic energy of the particle is below the threshold of 100 MeV for gammas and electrons, and 10 MeV for hadrons and

muons. For hadronic interactions with atmosphere, Helium nuclei are modelled as a bag of 4 independent nucleons each carrying one fourth of the total energy (commonly known as "superposition scheme"; one of its justifications can be found in the results of He-p total cross-section at high energy which has been measured at the CERN ISR[18] and found to be 4 times the p-p total cross-section.) In the interaction of protons or helium nuclei with atmosphere, neutrinos produced are assigned the right flavour according to their parent particle's nature and tracked forward to the Earth surface. Muons are also tracked down to the Earth surface for comparison with ground level muon measurements.

For the detection, AMS is represented by a spherical layer at an altitude of 380 km. Particles are counted as detected if they cross this layer with an incidence angle with zenith smaller than 32 deg. for protons, and 25 deg. for electrons and positrons. This corresponds to the AMS experimental angular acceptance. Particle spiralling in the magnetic field are counted as many times as they cross the surface within the acceptance angle. Statistical error calculation takes into account the fluctuations induced by particles with very high weight due to multiple detection.

It is worth mentioning that a global factor of 3 in computing time is saved by using method A instead of method B.

### 3 Results on charged particles

The above simulation gives a complete set of prediction on particles fluxes, either primary or secondary, while using only as input the AMS rigidity spectra measured at the highest geomagnetic latitude. The dependence with geomagnetic latitude of the cutoff on energy spectra shows up very clearly (see fig.8 for primary protons energy spectra at 380 km in altitude). Secondary particles coming out from interaction of primaries on the atmosphere produce a second flux below the geomagnetic cut-off. Most of these interactions occur at an altitude close to 40 km (fig.6), which is a trade-off between high enough atmosphere density for primary particles to interact and low enough atmosphere density to avoid absorption of outgoing secondary particles before their detection at 380 km. For neutrinos which come from the decay of secondary pions, muons and kaons the probability of interaction of primaries is dominant and thus the mean altitude of production is much smaller, about 18 km (fig.15). Near the geomagnetic equator the secondary flux of charged particles detected at the AMS altitude is about doubled. Such excess with respect to higher geomagnetic latitudes is due to the Earth magnetic field and to its anomalies, in which secondary particles produced in the atmosphere are brought to higher altitude by following the field lines; they can oscillate East-West and bounce North-South while spiraling around the field lines. This creates a kind of ring of charged particle around the altitude of AMS with an energy as high as 6 GeV. This was observed by AMS for protons, electrons, positrons, and helium as well.

Fig.7 compares the proton kinetic energy spectra measured by AMS with the result of this work, as a function of geomagnetic latitude. The agreement is remarkable enough, though only one normalization constant is used for all absolute fluxes, namely the flux of protons at 100 GeV measured by AMS. Fig.8 exhibits the part of the spectra due to primaries. As expected, there is almost no particles below the geomagnetic cut-off, which is not the case for some other works like ref.[19] for instance.

Comparison of electron and positron spectra with AMS measurements are shown in figures 9 and 10. The agreement is pretty good for geomagnetic latitudes from 0.3 to 1., with both simulation and real data showing up the appearance of primary lepton flux

above cut-off in downwards particles. Differently enough, in the bin 0.0 to 0.3 the measured flux of electrons and positrons is in excess by a factor up to 6 at low energy with respect to Monte-Carlo prediction. It is worth noting that such discrepancy is also present in other simulation works [20]. Although we cannot explain with certainty this discrepancy, some approximations done in the simulation are likely to contribute to that. First, the atmosphere density at high altitude (above 50 km) varies by a factor up to 3 with latitude (fig11), which can induce a sizeable change in the mean life-time of the trapped electrons or positrons. Second, it is not possible in the simulation to trace highly oscillating trapped particles until the end of their path, which implies an underestimation of their statistical weight. Eventually, let's remark the difference in absolute flux for upward going and downward going particles in the experimental data while there is no such difference in the Monte-Carlo data; if most particles are trapped, upwards and downwards fluxes should be equal.

The ratio of secondary positron to electron yield, shown in fig.12 as a function of geomagnetic latitude, is in very good agreement with AMS data. It exhibits the remarkable feature of varying from about 4 at the geomagnetic equator down to 1 near the poles. If the Earth magnetic field is switched off in the simulation, or if the primary flux is restricted to gamma rays, then this effect disappears. It can thus be deduced that this anomalous ratio measured in the geomagnetic equatorial region is due to the effect of the Earth magnetic field on the acceptance of both primary and secondary particles. Selecting primary protons above 30 GeV gives a ratio of only 2 at the equator, pointing out the role of the primary proton energy in this anomaly.

This simulation allowed us to calculate the flux of muons at ground level and to compare it to the experimental data taken by the CAPRICE experiment[21] in 1994 at Lynn-Lake ( Manitoba, Canada). This is a direct test of the capability of this simulation to predict neutrino fluxes, since muons and neutrinos are directly correlated. To take into account the experimental conditions and the detector acceptance, muons have to be in the geomagnetic latitude range of 64.4-67.3 deg. and to impinge on ground with an angle smaller than 12 deg. with respect to zenith. To get enough statistics, we integrated on longitude. The difference of solar activity between June 1998 ( AMS) and July 1994 ( CAPRICE) as measured by the CLIMAX neutron monitor[22] (fig.13) is small enough to neglect its effect on the spectrum of primary protons. Fig.14 shows the comparison between experimental and simulated muon data. The agreement is pretty good both in shape and in absolute flux, though there is no free parameter in the simulation.

## 4 Atmospheric neutrinos: general features

The above result on muons is a powerful test of the reliability of the simulation of neutrinos in our model. As stated above, both the propagation of primary particles and the development of the hadronic shower have effect on neutrino distributions. The magnetic field induces a correlation between position and direction of charged particles which in turn correlates the various distributions of neutrinos. For the sake of comparison, many plots shown below are using the same variables and cuts than those used by other authors. Distributions are shown in 3 latitudes slices ( in radians: 0.-0.2, 0.2-0.6, 0.6-1.) and in 4 neutrino momentum ranges( in GeV: 0.1-0.31, 0.31-1.,1.-3., 3.1-10.). We call " zenith angle " the angle between the zenith direction in a given point and the direction of a neutrino arriving at this point ( thus, a neutrino going in direction of the Earth's center has a zenith angle of 180 deg.).

Fig. 15 shows the altitude of production of neutrinos from pion and muon decays. On average, neutrinos from muon decay are produced 2 km lower in altitude, due to the longer lifetime of muons. Near the geomagnetic poles, neutrino flux is higher by about a factor 2 at low energy, which is related to a higher primary proton flux corresponding to the lower geomagnetic cut-off present in these regions ( fig.16). The predictions on zenith angle of neutrinos are shown in fig.17 to fig.19. There is a good compatibility in shape with some previous works [6, 23, 24], though there is differences on amplitudes. This could come for instance from the simulation of hadronic cascades, but further work is needed to identify precisely the origin of these differences. An enhancement of the zenith angle distribution is seen at 90 deg. in all plots. Such effect was not present in former simulations using a 1 dimension approximation. The azimuth distributions are shown in fig.20 to fig.22. In all these plots, asymmetries fade out when energy increase, reflecting also the higher energy of the parent primary, less and less sensitive to magnetic field effects.

Last, fig.23 to 25 show the ratio of muonic to electronic neutrinos  $(\nu_\mu + \bar{\nu}_\mu)/(\nu_e + \bar{\nu}_e)$  for the same latitude and energy bins. The strong zenith angle dependence which shows up is due to the correlation between this angle and the path length of parents particles. Compared to other works [23], we find a smaller ratio in the vertical direction ( zenith angle near 0 or 180 deg.). As an example, this ratio goes only up to 3.5 in our data ( energy slice 3.1-10. GeV, latitude 0.2-0.6 rad.) while [23] gets a value of 4.2.

#### 4.1 Results in the Super-Kamiokande region

The Super-Kamiokande region is approximated by a slice in geomagnetic latitude covering  $\pm 5$  deg. around the geographic location of the Super-Kamiokande (S.K.) experiment. The flux is integrated on longitude to get more statistics. We checked that there is no visible difference when the longitude is restricted to  $\pm 30$  deg. around the S.K. one.

In S.K., the neutrino variables are deduced from the measurement of the charged lepton produced in the interaction with the sensitive medium. The reconstruction accuracy is pretty poor below 1 GeV. To take the measurement error into account, the neutrino direction generated is smeared [25, 26] according to the law  $40^\circ/\sqrt{E_\nu}$  to get the outgoing lepton direction, while for the lepton momentum a flat random generation between  $0.25 \times E_\nu$  and  $E_\nu$  is used. The S.K. detection Monte-Carlo would be necessary for getting a better approximation. To normalize our data to the number of events in S.K., the simulated events are weighted by the cross-section of neutrinos on the sensitive medium, which at very low energy is only poorly known[27]. The effect of smearing can be seen in comparing figures 31 and 32 which show zenith angle distribution for two energy ranges. For the lower energy bin, peaks are washed out when smearing is applied.

The fig.26 shows the simulated neutrino fluxes multiplied by  $E_\nu^{2.5}$ . Here we use for the sake of comparison the weights corresponding to primary spectra used by Honda et al.[1]; the agreement between our result and the first results of Honda et al.[1] and Bartol group[2] is very good. In figure 27, we use AMS primary spectra as we did above, with a solar modulation correction corresponding to years 1996,97, and 98 ( see fig.28). The results of other works ([1],[4],[23]) are also shown. Contrary to the previous figure, our results in fig.27 are sensibly higher than the other ones for energies below 0.4 GeV, while the agreement is good for higher energies. We are in general 20% higher in flux than the recent results of G. Battistoni et al.[4]. To test the sensitivity of these spectra to the solar modulation, we calculated the neutrino energy spectra with the parameters corresponding to years 1999 to 2001. The ratio of the former predicted fluxes to these new ones is as

high as 10% at low energy, going down to 5% above 1 GeV. As for the rest of this paper, the Honda's parametrization [1] of the solar modulation is used.

The ratio of fluxes (up-down)/(up+down) for muonic and electronic neutrinos is shown in fig.30. Events with zenith angle in the range  $-0.2$   $+0.2$  are not used. In the top histograms, events generated are not smeared, while bottom ones are smeared for lepton measurement according to the formulae described above. Unsmeared muonic neutrino data are in quite good agreement with the recent work of G. Battistoni[5]. The good agreement between our prediction and S.K. data for electronic neutrino, and the very bad one for muonic neutrino confirm the evidence for a muonic neutrino disappearance. Fig. 32 shows the comparison between data and Monte-Carlo for the zenith angle distribution for the "sub-GeV" class of events and the "multi-GeV" one. Electronic-neutrino distribution is normalized to equal surface, while for muonic neutrinos the normalization is done only on the last 3 bins in zenith angle. Our distribution is in slightly better agreement than the results of previous works. This gives a hint about the sensitivity of the S.K. oscillation parameter result to the model used for simulation. However, it could be that this is dominated by the way the smearing is taken into account.

The ratio of fluxes of neutrino species is given in fig. 33 as a function of zenith angle. We have not been able to compare it with S.K. data since this apparatus has not the same acceptance for electrons and muon, the S.K. detector Monte-Carlo being necessary to evaluate them. Our ratio is smaller than in other works, which could lead to a change in the oscillation parameters calculated by S.K. with their simulation.

Also shown (fig.34) is the azimuthal distribution of neutrino species compared with S.K. data, in quite good agreement for electron-like type and exhibiting the so-called "East-West effect", and with some difference for muon-like neutrino events. ( we did not put  $\nu$  oscillation in our events to look for a possible explanation of this disagreement).

## 5 Conclusion

A model of simulation of the effect of interaction of primary cosmic rays with the Earth atmosphere has been developed. Based on the GEANT3 package together with its GFLUKA option for hadronic interactions, and using the primary energy spectra measured in AMS as input, this work was able to reproduce pretty well all the distribution measured in AMS, while using the proton flux at 100 GeV measured by AMS as unique normalization constant. The difference on the absolute flux of leptons predicted at the geomagnetic equator is likely to have its origin in the variation of atmosphere density with geographic latitude which is not taken into account in this work. However the effect is sizeable only at low energy.

This work has allowed also to predict fluxes of neutrinos from interaction of primary cosmic rays on atmosphere. The good agreement between the prediction on muon fluxes at ground level and the measurements of the CAPRICE experiment demonstrates that the neutrino simulation is reliable and accurate. It is compatible with most of the other simulation work within 20%. The agreement with the Super-Kamiokande e-type neutrinos data is quite good, while a clear discrepancy is observed for muon-neutrinos, as expected from neutrino oscillation. As a conclusion, the secondary flux of particles observed by AMS does not affect the conclusion of the Super-Kamiokande experiment about neutrino oscillations. However, the slight differences observed between the results of this work and those of the other authors indicate the kind of room left for systematic error on

the proposed oscillation parameters; but this needs the S.K. apparatus simulation to be precisely evaluated.

## 6 Acknowledgements

We would like to thank L. Derome, F. Donato, M. Maire and N. Produit for helpful discussions.

## References

- [1] M. Honda et al., Phys.Rev. D52 (1995) 4985.
- [2] T.K. Gaisser et al., Phys.Rev. D38 (1988) 85.
- [3] V. Agrawal et al., Phys.Rev. D53 (1996) 1314.
- [4] G. Battistoni et al., hep-ph/0207035 v1 (2002).
- [5] G. Battistoni et al., hep-ph/0012268 v2 (2002).
- [6] P. Lipari, Astropar.Physics 14 (2000) 153.
- [7] A.M.S Collaboration, Phys. Lett. B461 (1999) 387-396.
- [8] A.M.S Collaboration, Phys. Lett. B472 (2000) 215-226.
- [9] A.M.S Collaboration, Phys. Lett. B484 (2000) 10-22.
- [10] A.M.S Collaboration, Phys. Lett. B494 (2000) 193-202.
- [11] A.M.S Collaboration, Physics Reports v366 (2002) 331-405.
- [12] M. Boesio et al., Astrophys. J. 518 (1999) 457.
- [13] T. Sanuki et al., Astrophys.J. 545 (2000) 1135.
- [14] J. Favier, AMS analysis meeting, 26 Nov. 1999.  
<http://ams.cern.ch/AMS/Analysis/acorner.html> J.Favier," Geant dans l'Espace ",  
talk given at the LAPP workshop, Aussois 2-3 Dec. 1999 (un-published)
- [15] MSIS-E-90 Atmosphere Model  
[http://nssdc.gsfc.nasa.gov/space/model/models/msis\\_n.html](http://nssdc.gsfc.nasa.gov/space/model/models/msis_n.html)
- [16] T. K. Gaisser et al., Proceedings of ICRC 2001: 1643 Copernicus Gesellschaft 2001.
- [17] GEOPACK-1994  
Nikolai A. Tsyganenko, Geomagn. and Aeronomy V26 (1986) 523-525.  
N.A Tsyganenko et al., Soviet Geophys.Comm., Moscow, 1987.  
See references and web sites in: " A geomagnetic Field Model For Alpha Magnetic Spectrometer Data Analysis" Ming-Huey A. Huang, AMS note AMS-1998-10-29.



- [18] see for example, the M.A. Faessler's presentation on ISR results in proceedings of the 17th Rencontre de Moriond, Second session, Les Arcs 1982 , editions Frontieres , J. Tran Than Van, editor.
- [19] V. Plyaskin, Phys.Lett. B516 (2001) 213.
- [20] L. Derome et al., Phys.Lett. B 515 (2001) 1.
- [21] J. Kremer et al., Phys.Rev.Lett. 83 (1999) 4241.
- [22] University of New Hampshire; <http://ulysses.sr.unh.edu/NeutronMonitor>
- [23] Y. Liu et al., Phys. Rev. D67 (2003) 073022.
- [24] M. Honda et al., Phys.Rev. D64 (2001) 053011.
- [25] John G. Learned " The Atmospheric Neutrino Anomaly: Muon Neutrino Disappearance " hep-ex/0007056 v1 (2000).
- [26] H. Sobel, " Atmospheric Neutrinos in Super-Kamiokande ", Proceedings of the XIXth Int.Conf. on Neutrinos Physics and Astrophysics, Sudbury, 16-21 June 2000; Nucl.Phys. B (proc suppl) 91 (2001) 127.
- [27] P. Lipari et al., Phys.Rev.Lett. 74 (1995) 184.
- [28] Super-Kamiokande Collaboration, Phys.Rev.Lett. 81 (1998) 1562.
- [29] Super-Kamiokande Collaboration, Phys.Rev.Lett. 82 (1999) 5194.
- [30] M. Shiozawa, " Experimental results on atmospheric neutrinos in Super-Kamiokande ", NEUTRINO-2002, May 25-30, 2002, Munich, Germany.  
<http://neutrino2002.ph.tum.de/pages/transparencies/shiozawa>

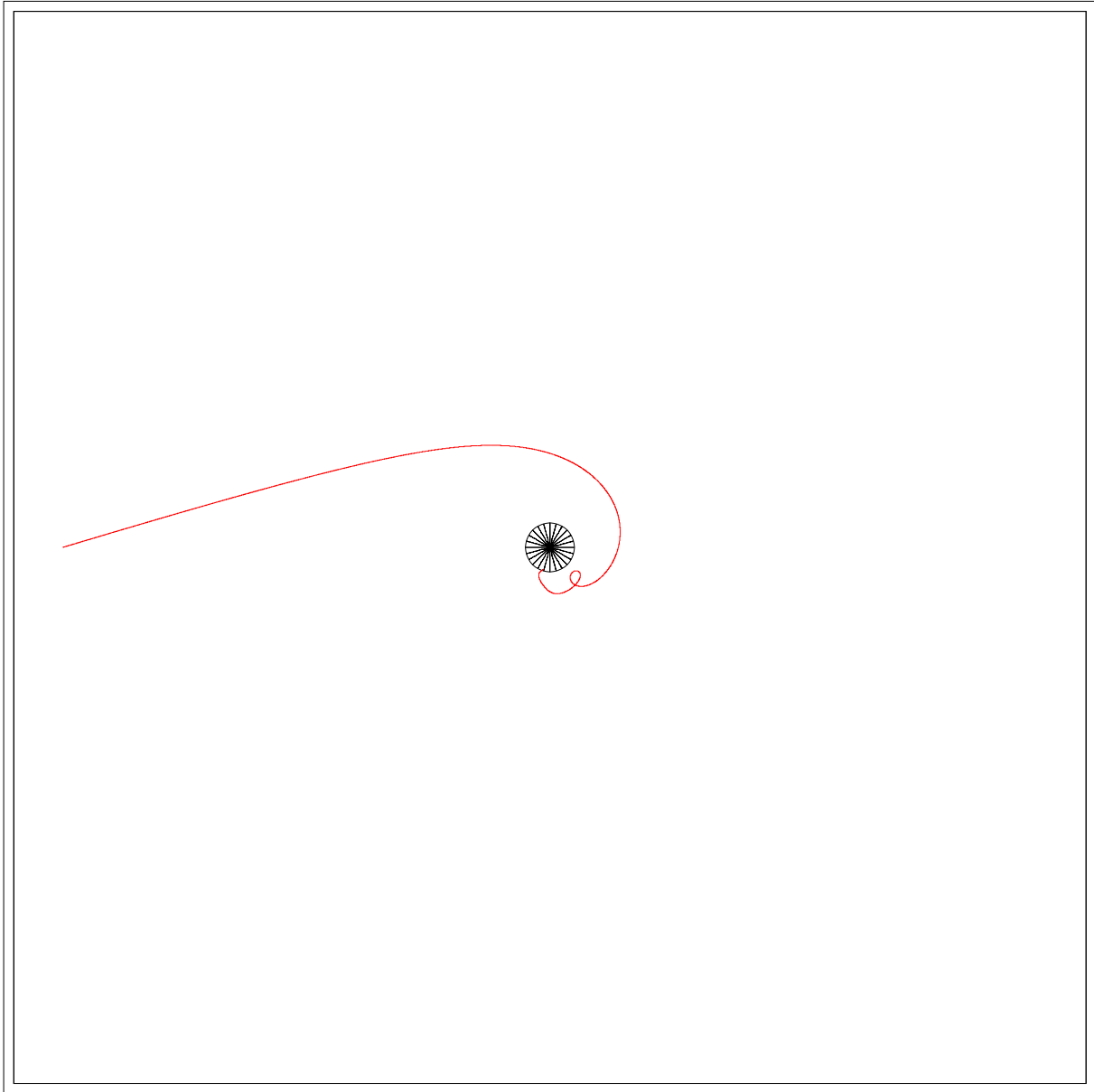


Figure 1: Trajectory of a 5 GeV proton generated with an impact parameter of  $6R_0$ , but nevertheless reaching Earth. Generation far from Earth (method B) requires such large aperture generation cones leading to poor efficiency.

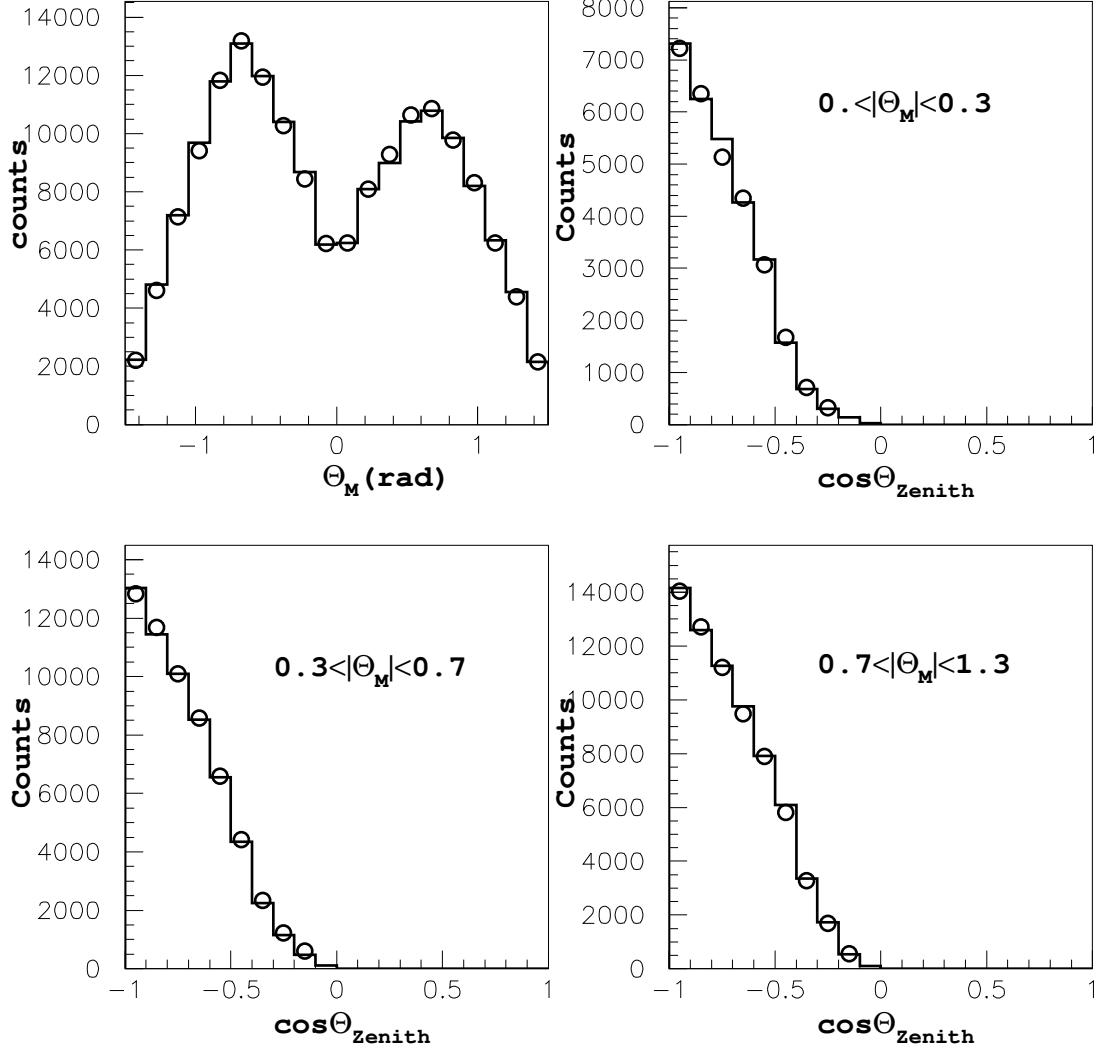


Figure 2: Comparison of generation far from Earth and near Earth ( open circles); (a) is the geomagnetic latitude population; the observed distortion of symmetry is a reflection of the difference of a dipole field and the real one which contains also the South-Atlantic anomaly. (b), (c), (d) are distributions of the zenith angle for three geomagnetic latitude bins. Positions and angles are computed at the 380 km altitude and here the proton energy range is 6-30 GeV.

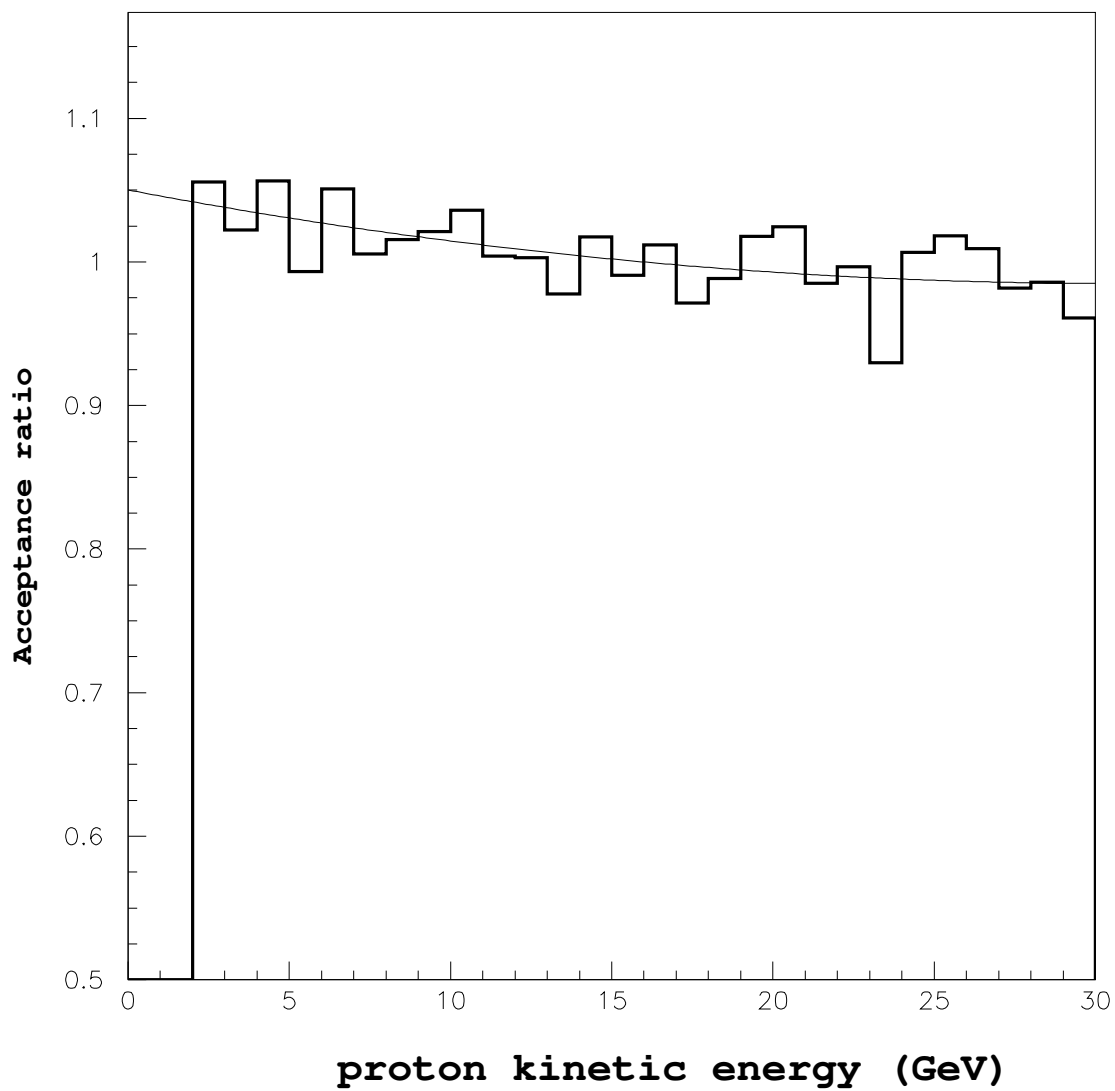


Figure 3: Ratio of acceptance between generating primary cosmic rays with an external sphere of  $10 R_0$  and  $20 R_0$ . The higher acceptance for the nearest distance means the presence of wrongly accepted trajectories.

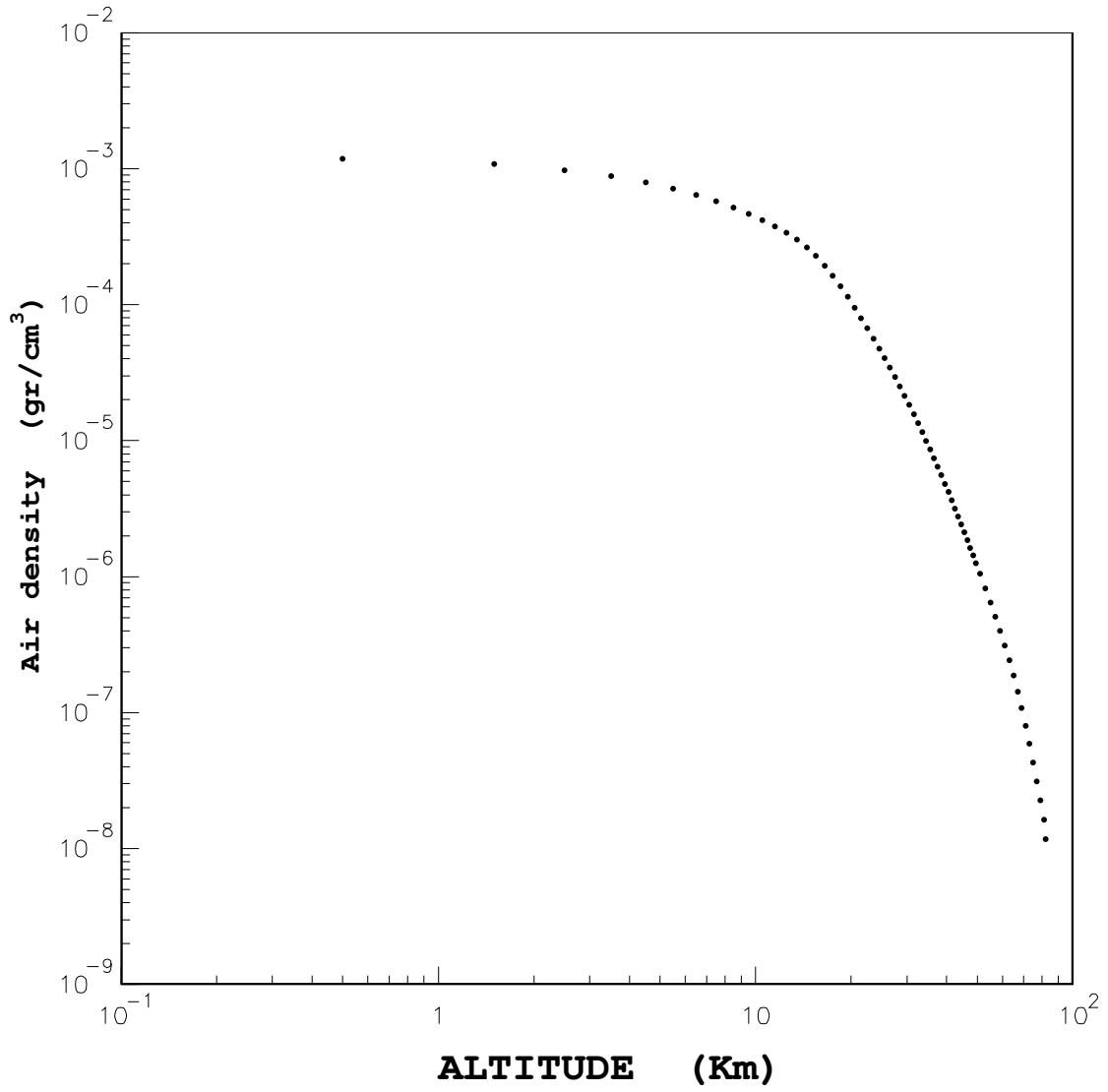


Figure 4: Air density as a function of altitude ( data from [15])

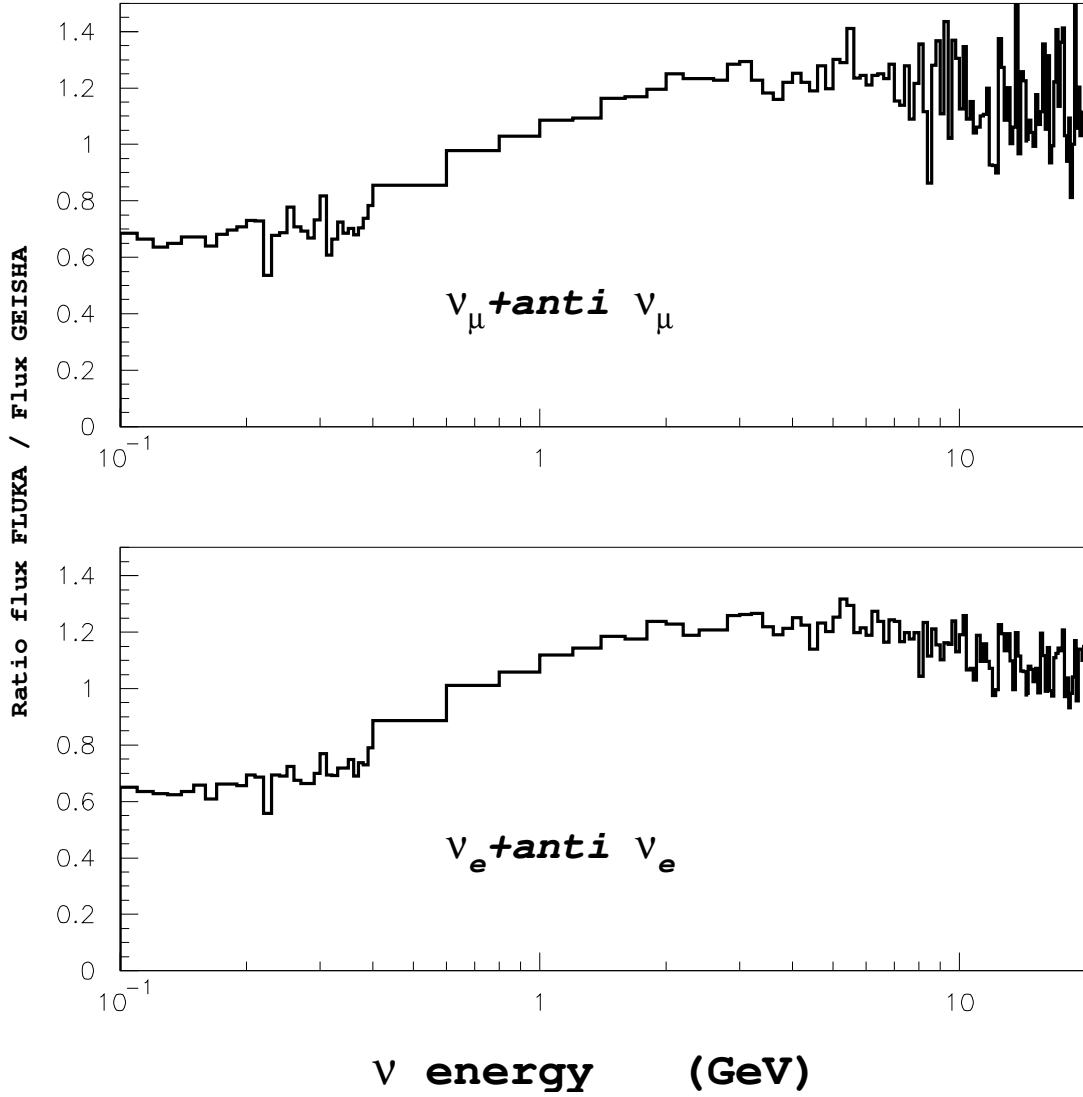


Figure 5: Ratio of atmospheric neutrino fluxes for a generation using GEANT3+GFLUKA package and a generation using GEANT3+GEISHA package as a function of neutrino energy for all geomagnetic latitudes.

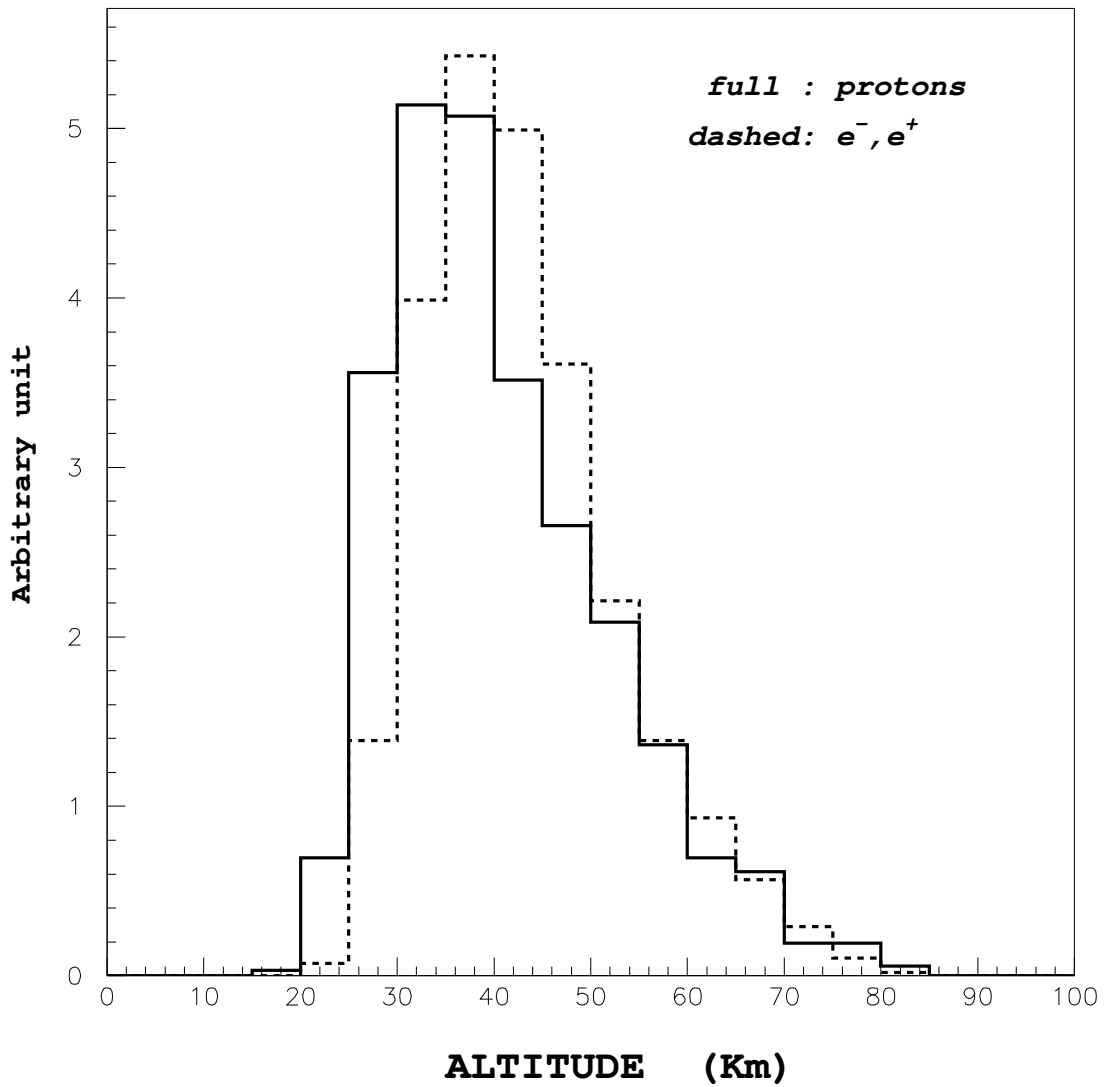


Figure 6: Production vertex altitude distribution for secondary protons and for electrons or positrons; average altitude is 41 km for secondary protons and 43 km for  $e^-$  and  $e^+$ . (These plots contain secondaries detected at the shuttle altitude with no angular acceptance cuts)

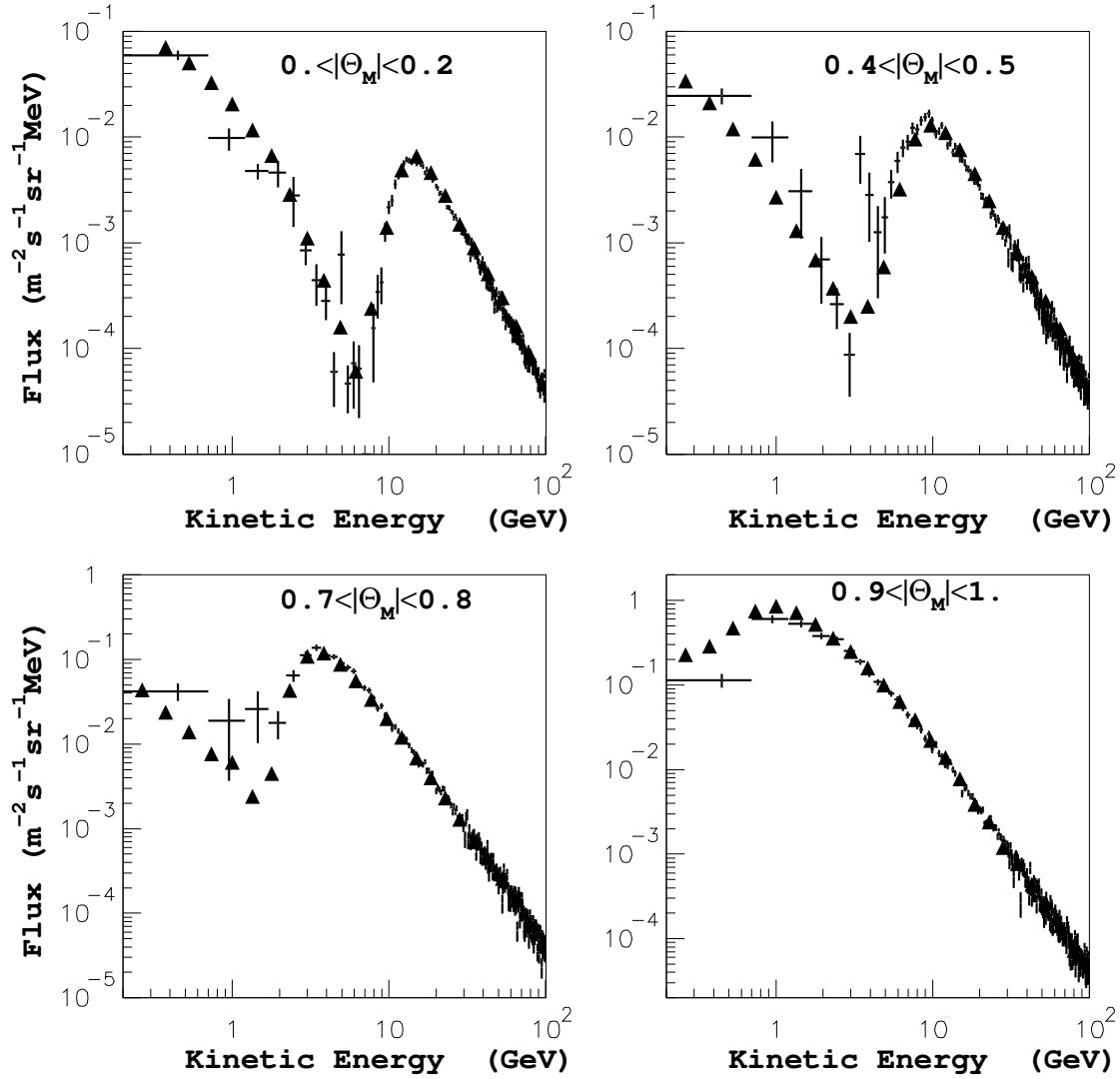


Figure 7: Comparison at different latitudes of AMS proton spectrum (black triangles) and this simulation. The MC spectrum is normalised once to the AMS data in the 100 GeV energy region.



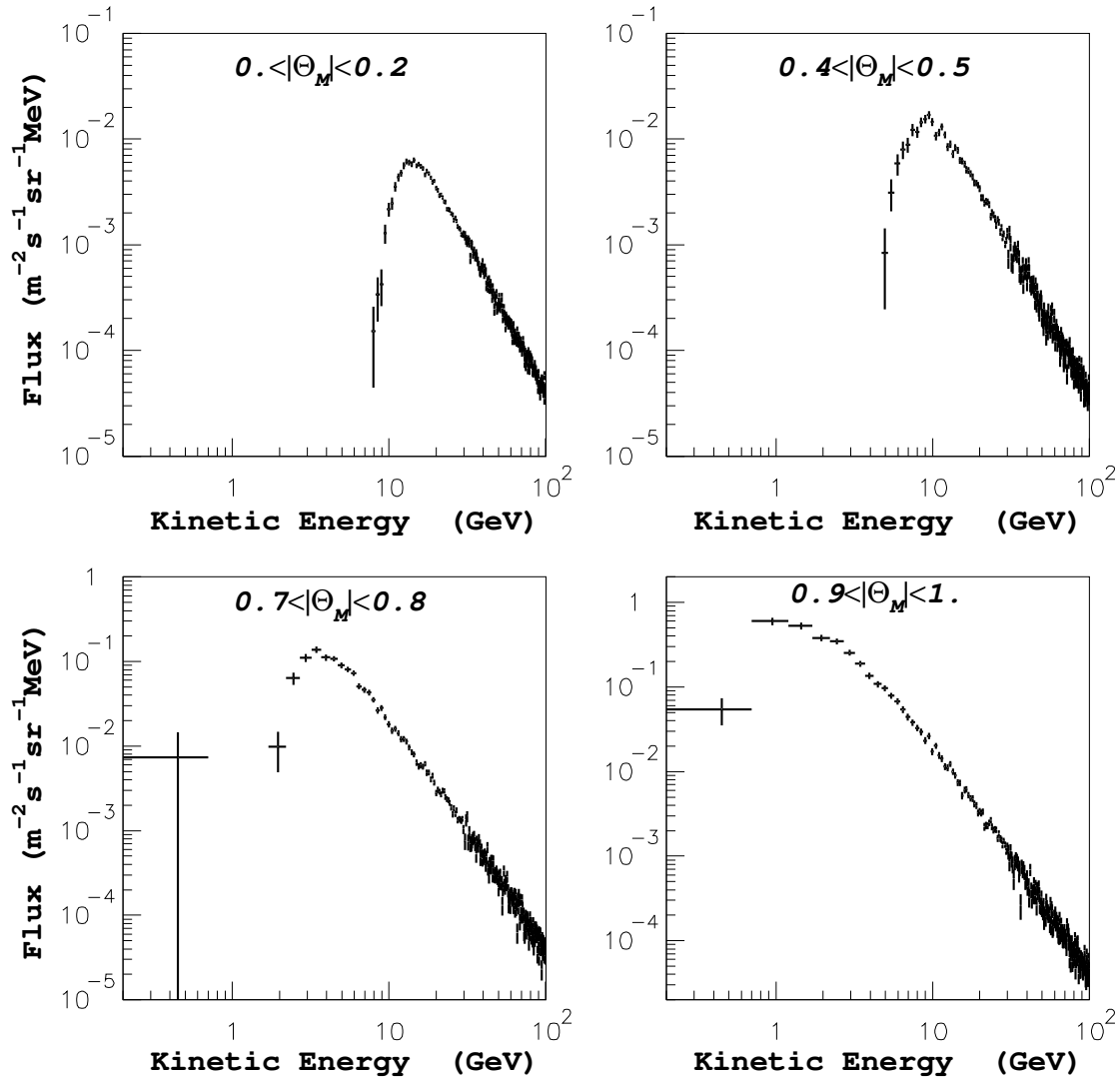


Figure 8: Same spectra as figure 7 in selecting only primary protons; the displacement of the geomagnetic cut-off with latitude is clearly seen.

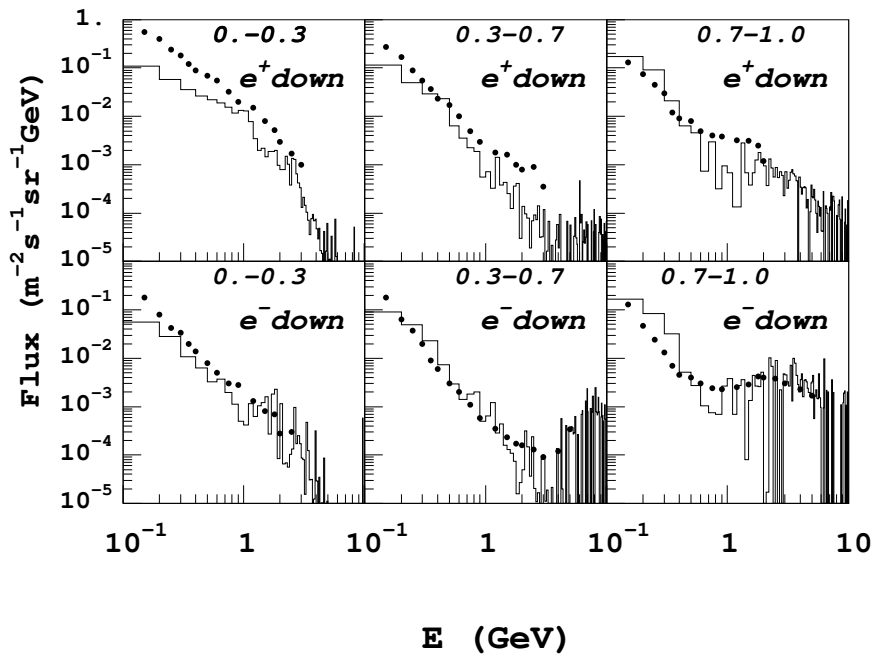


Figure 9: Downwards electron and positrons energy spectra for different geomagnetic latitudes; black dots are AMS data; notice the appearance of the primary electrons above cut-off.

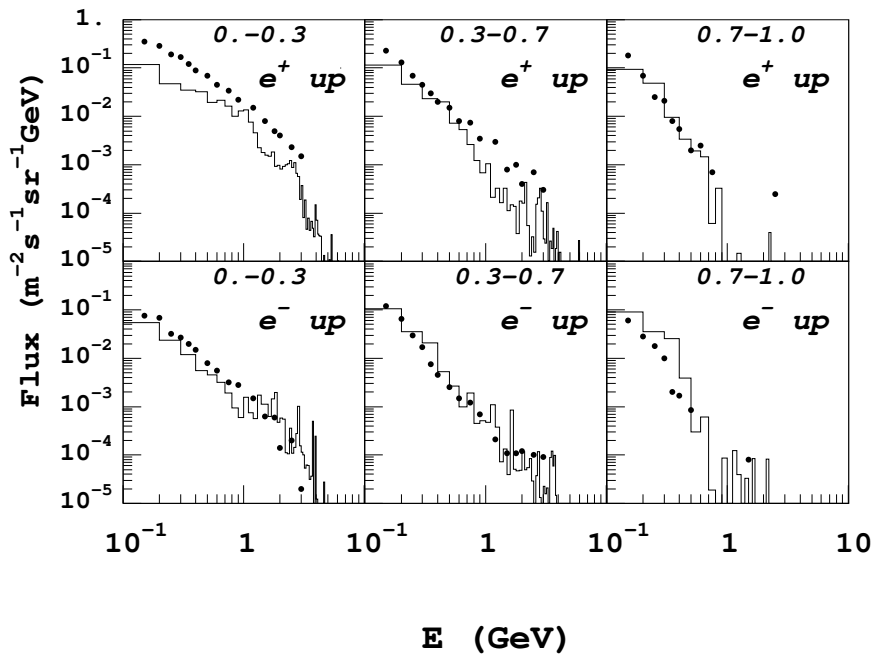


Figure 10: Upwards electron and positrons energy spectra for different geomagnetic latitudes; black dots are AMS data ( in its identification range)

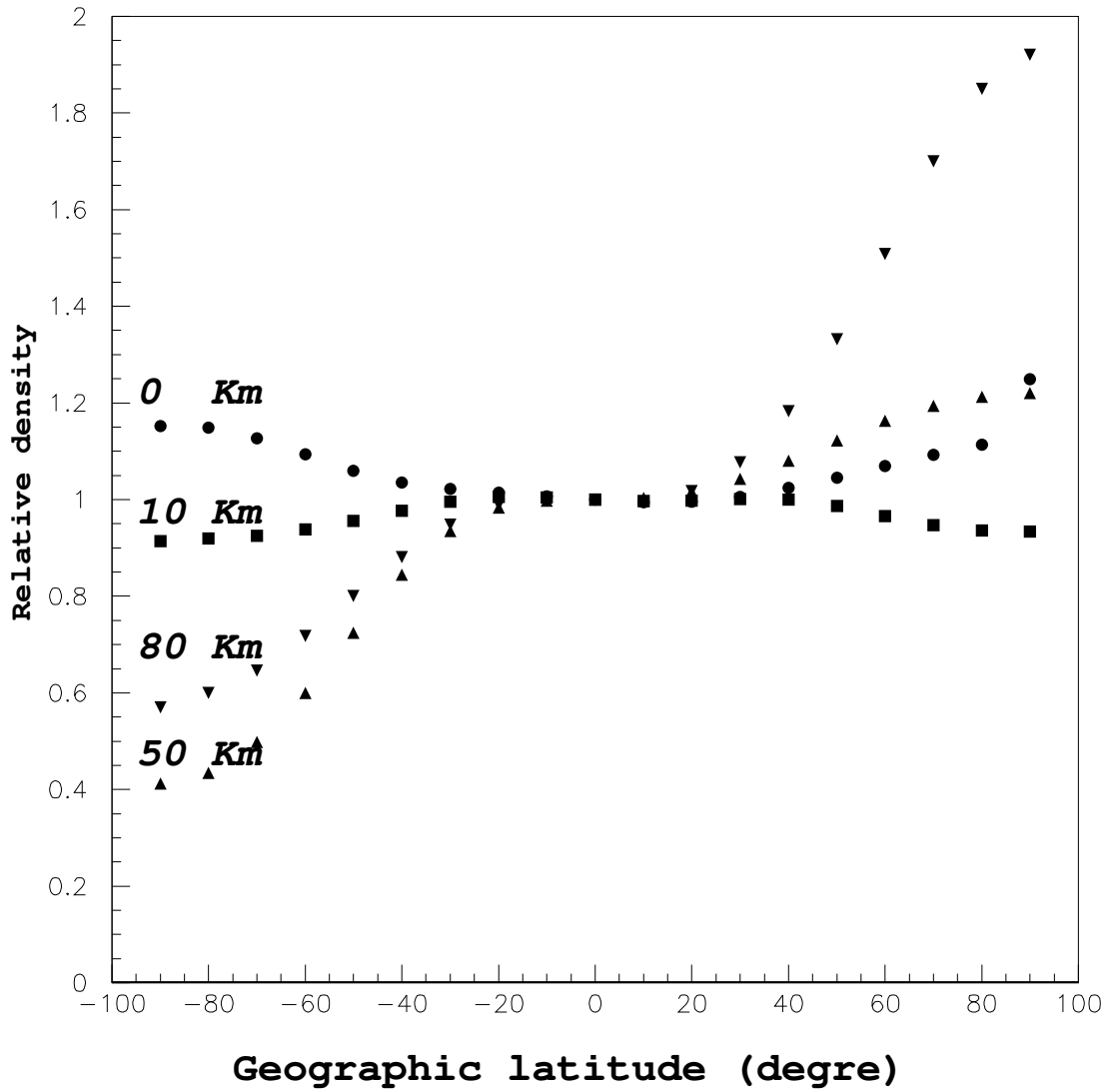


Figure 11: Variation of the air density with geographic latitude, for different altitudes. If the variation is limited to 30 % for low altitudes, it can reaches upto a factor 3 for the higher layers( data from [15]).

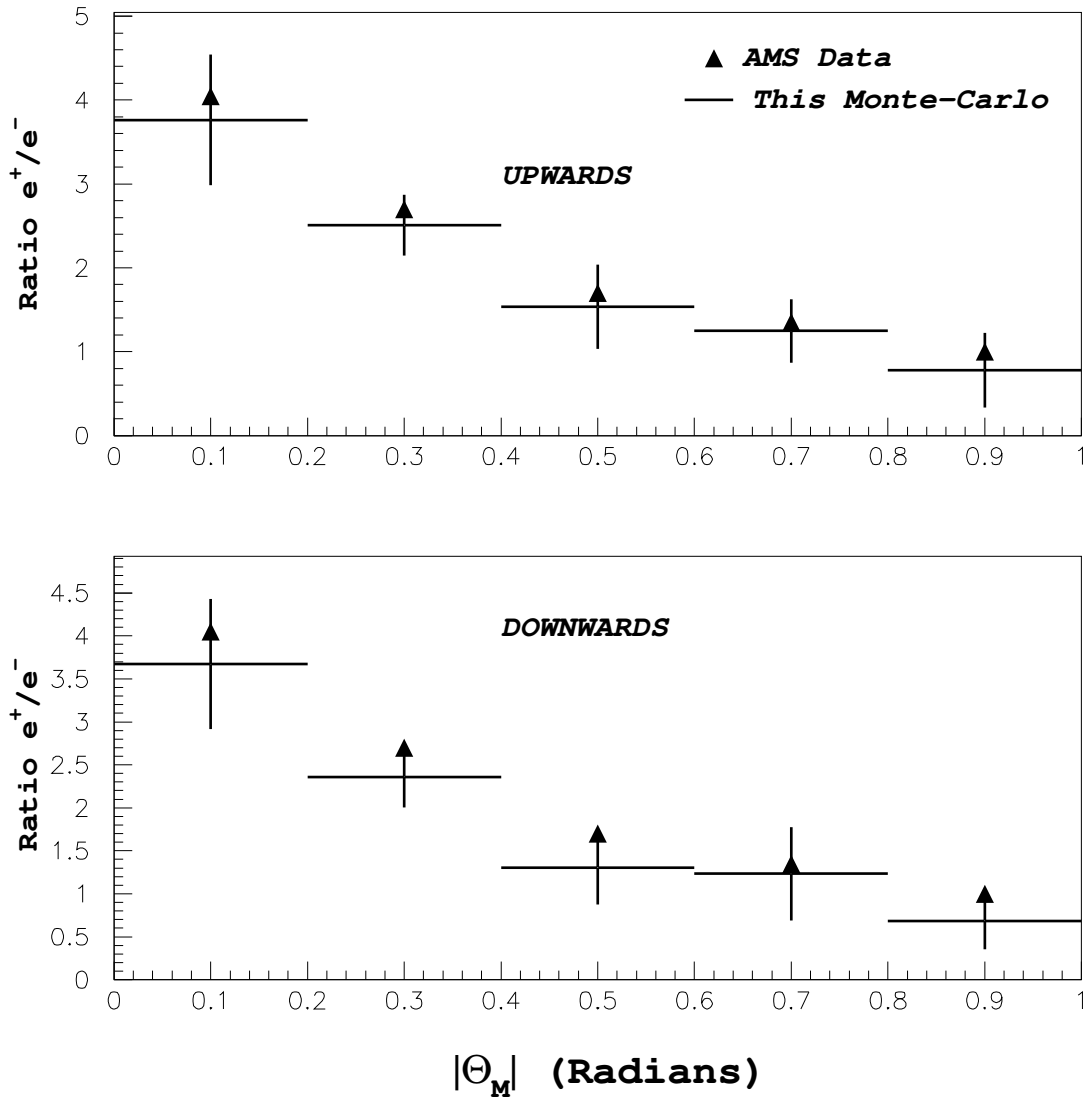


Figure 12: Evolution with geomagnetic latitude of the positron-electron yields ratio for upwards and downwards incoming directions.

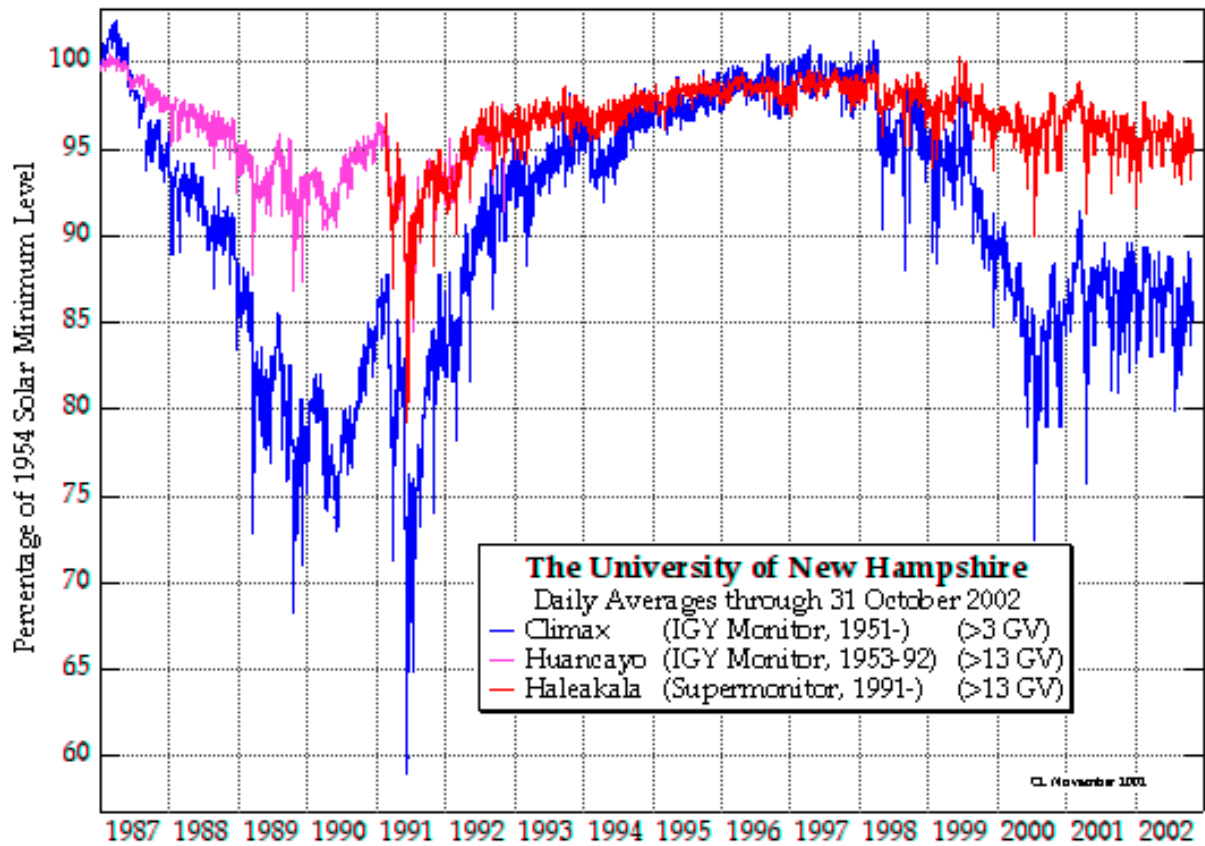


Figure 13: Solar activity as measured by the CLIMAX neutron monitor; one can see on the lower curve the small difference between June 1998 (AMS01) and July 1994 (CAPRICE) periods.

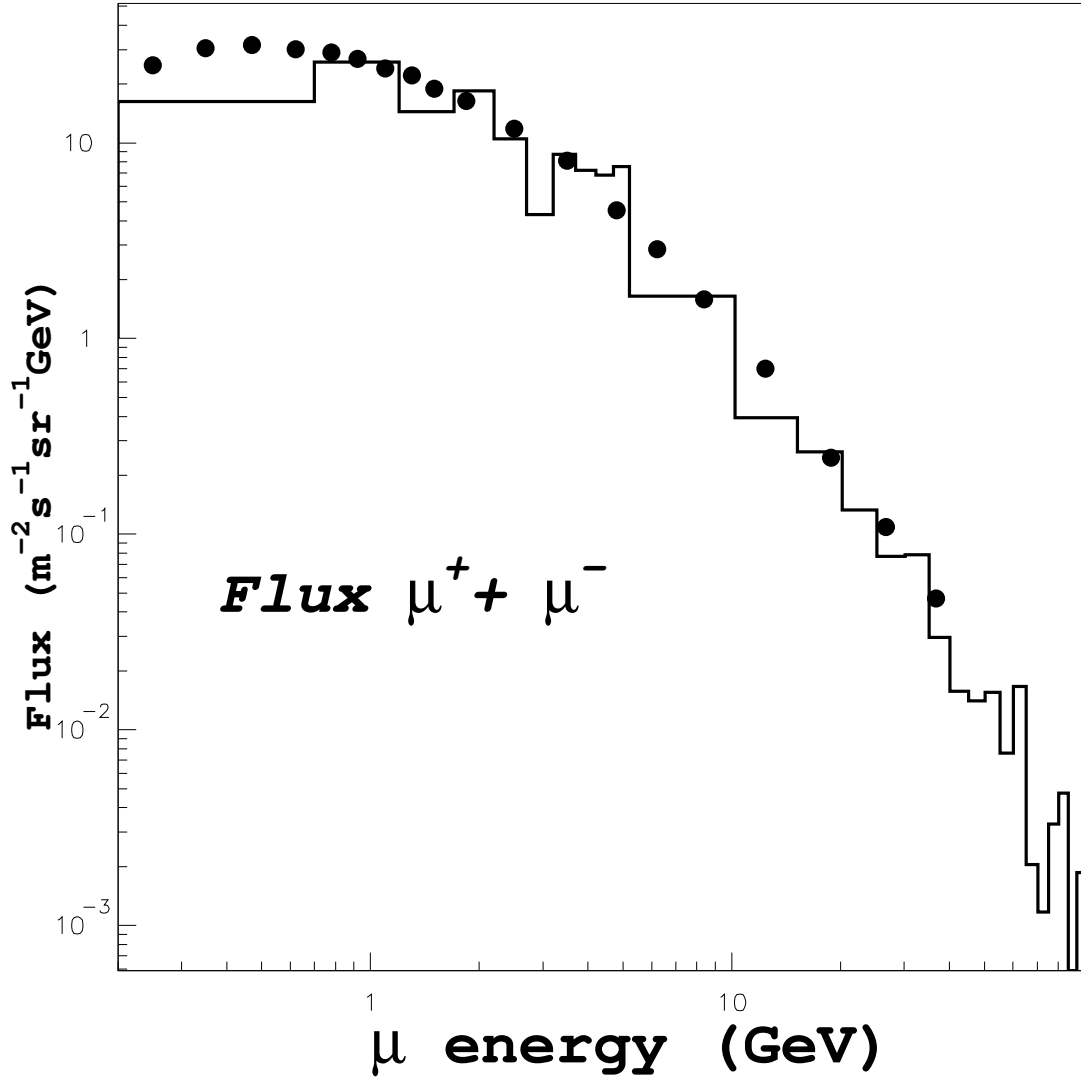


Figure 14: Muon spectrum of both charges measured at Lynn Lake by CAPRICE [21]( black circles); the histogram is the present simulation.

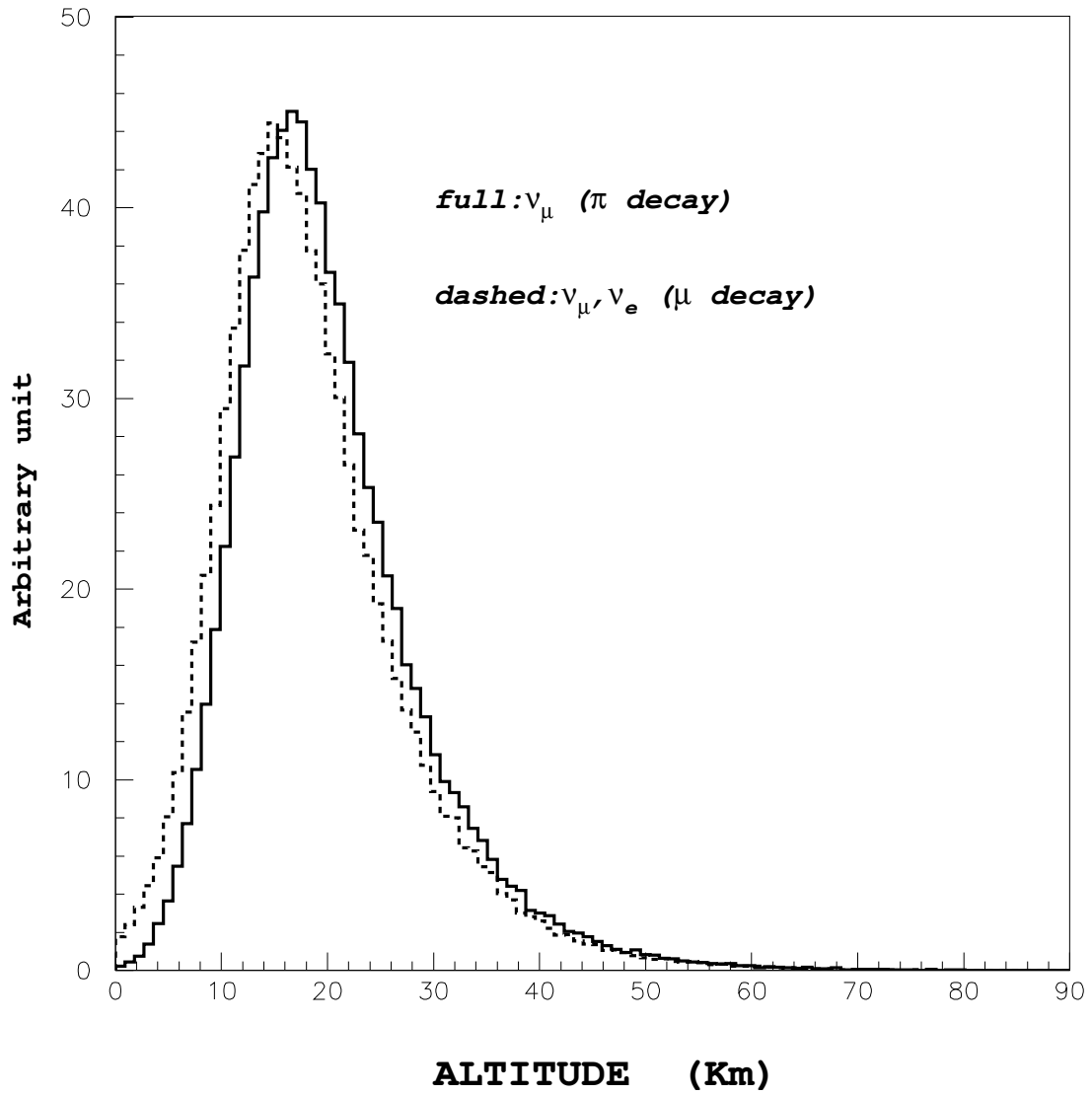


Figure 15: Production altitude of neutrinos issued from pions decays and muons decays



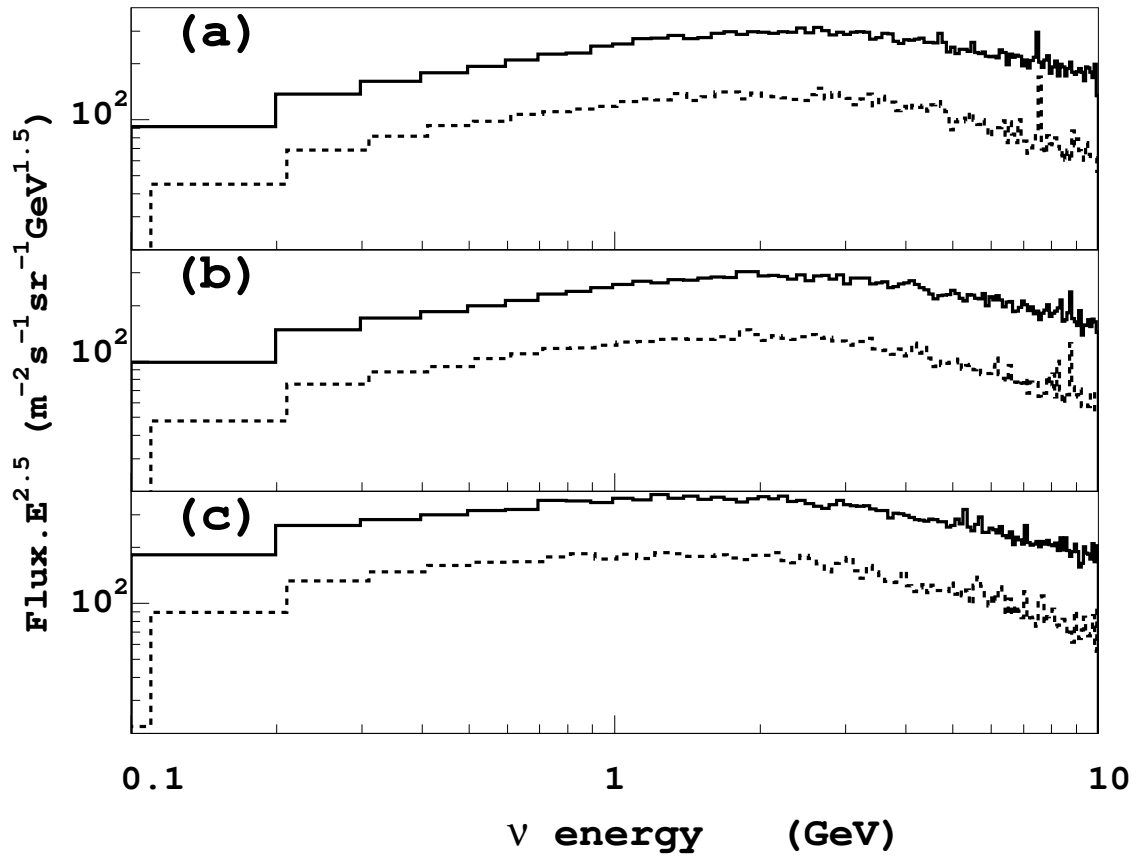


Figure 16: Neutrino fluxes averaged on angles for different geomagnetical latitudes: (a) 0.-0.2 rad, (b) 0.2-0.6 rad, (c) 0.6-1. rad. Full line histogram:  $(\nu_\mu + \bar{\nu}_\mu)$ . Dashed histogram:  $(\nu_e + \bar{\nu}_e)$

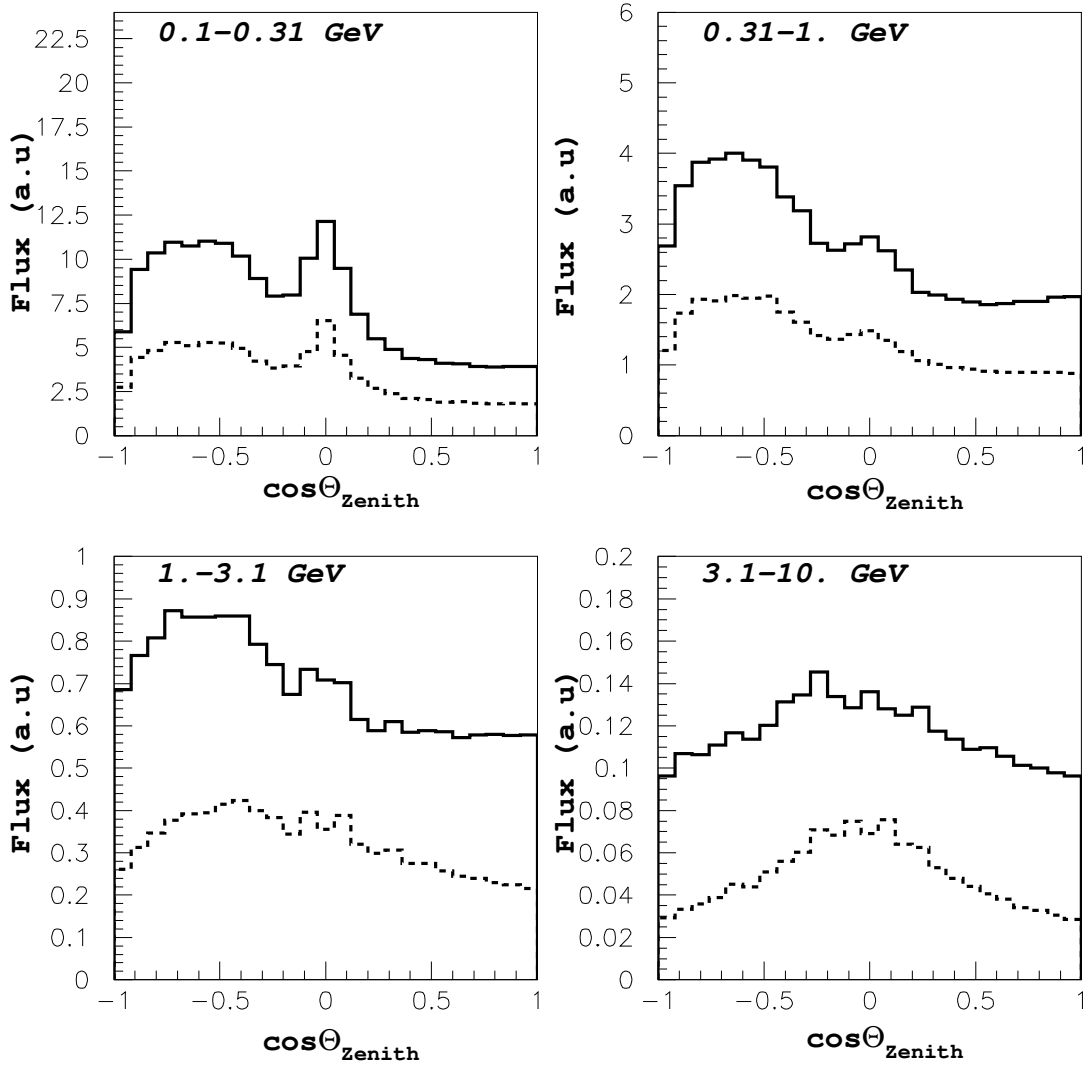


Figure 17: In the region of geomagnetical latitude  $|\Theta_M| \leq 0.2$  rad, zenithal angle distributions for 4 different neutrino momentum slices. Full line histogram:  $(\nu_\mu + \bar{\nu}_\mu)$ . Dashed histogram:  $(\nu_e + \bar{\nu}_e)$ .

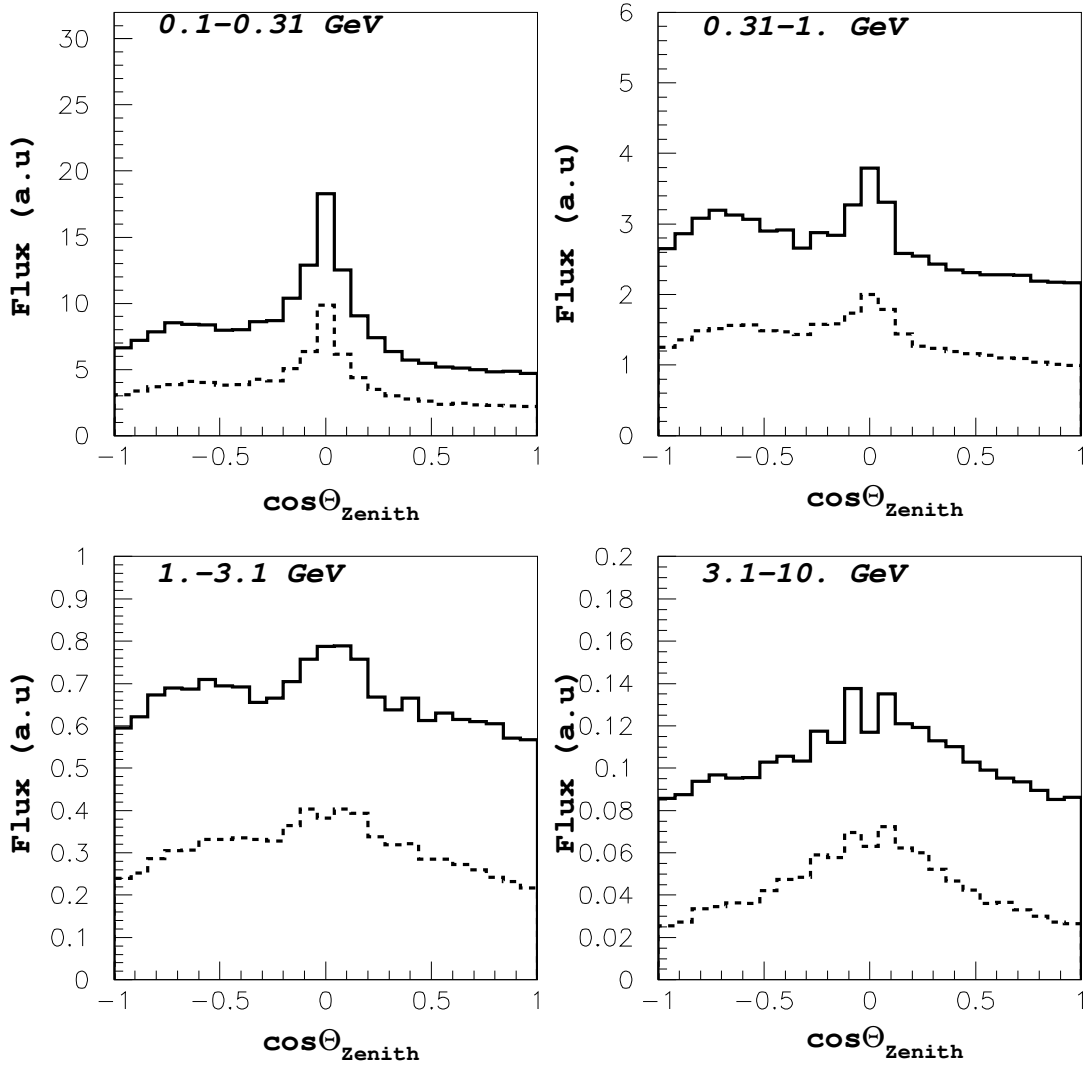


Figure 18: Same as fig.17 for the region of geomagnetical latitude  $0.2 \text{ rad} \leq |\Theta_M| \leq 0.6 \text{ rad}$ .

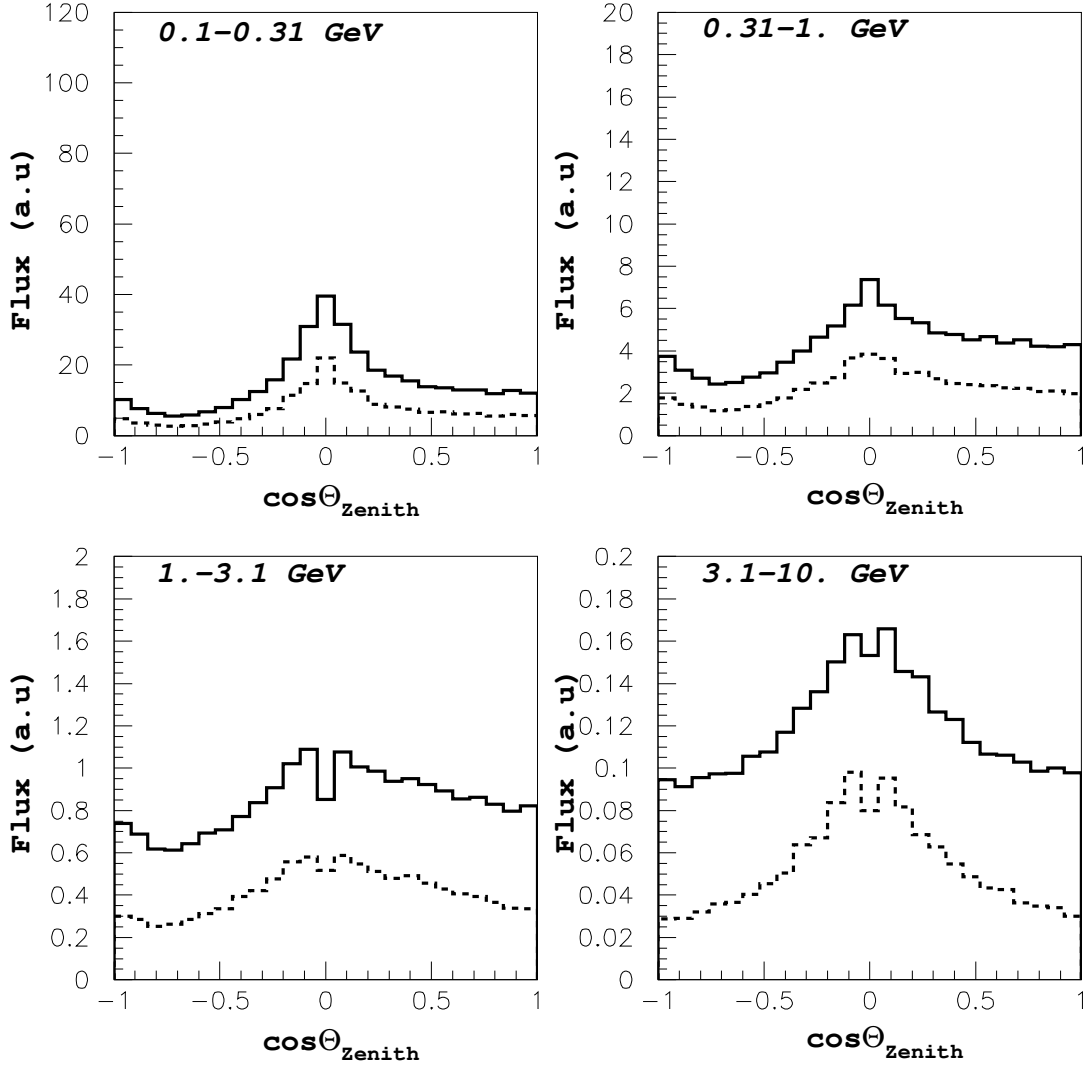


Figure 19: Same as fig.17 for the region of geomagnetical latitude  $0.6 \text{ rad} \leq |\Theta_M| \leq 1. \text{ rad}$ .

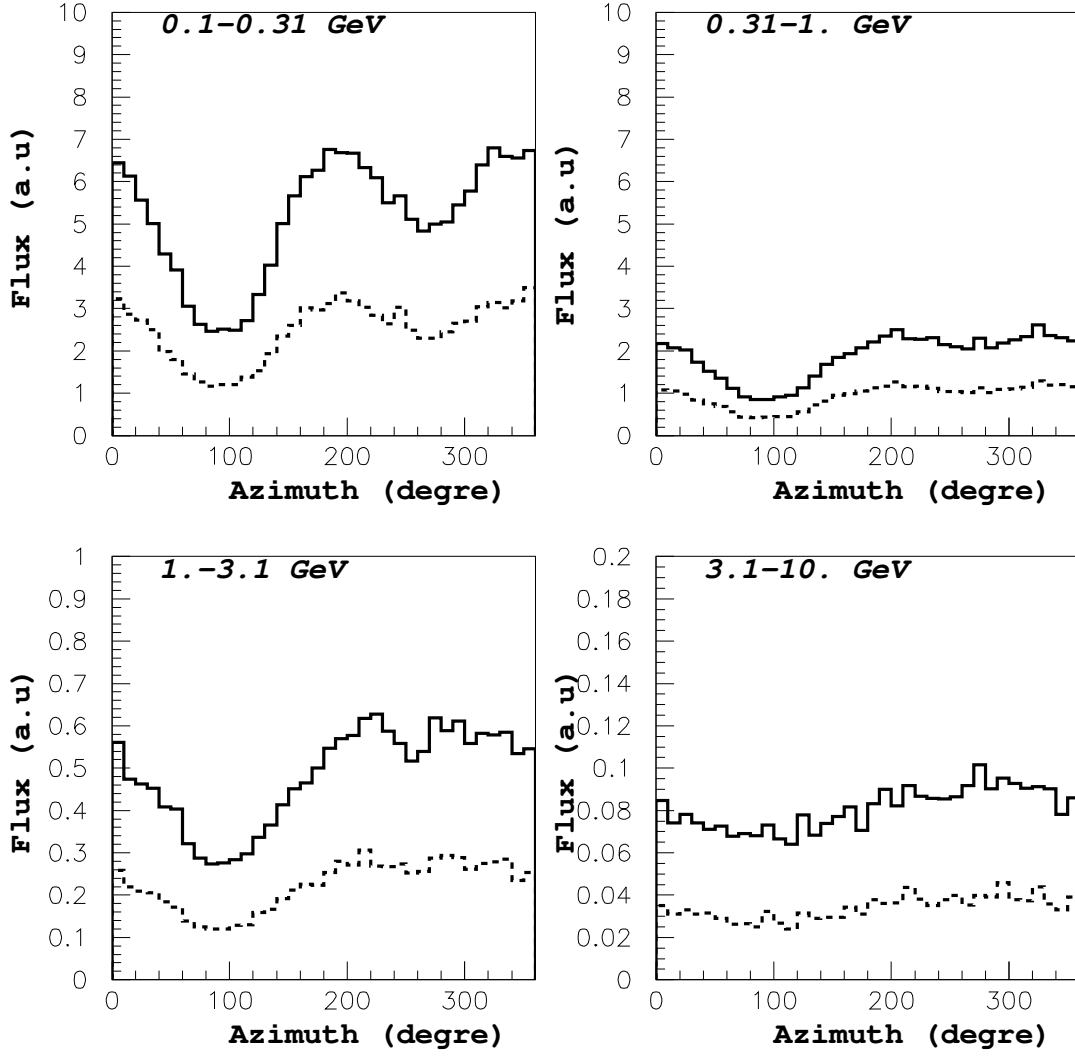


Figure 20: In the region of geomagnetical latitude  $|\Theta_M| \leq 0.2$  rad., azimuthal angle distributions for 4 different neutrino momentum slices. Full line histogram:  $(\nu_\mu + \bar{\nu}_\mu)$ . Dashed histogram:  $(\nu_e + \bar{\nu}_e)$ .

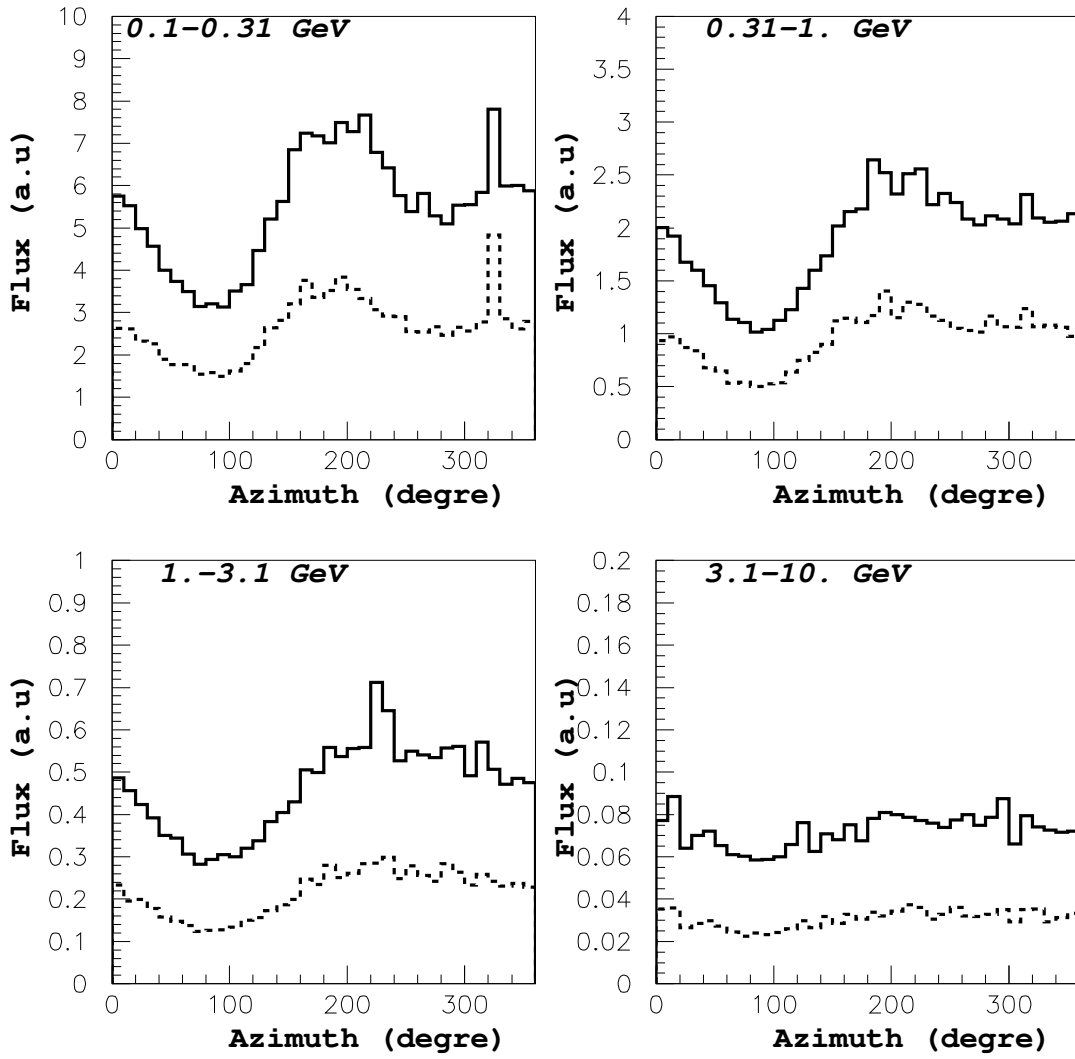


Figure 21: Same as fig.20 in the region of geomagnetical latitude  $0.2 \text{ rad} \leq |\Theta_M| \leq 0.6 \text{ rad}$ .

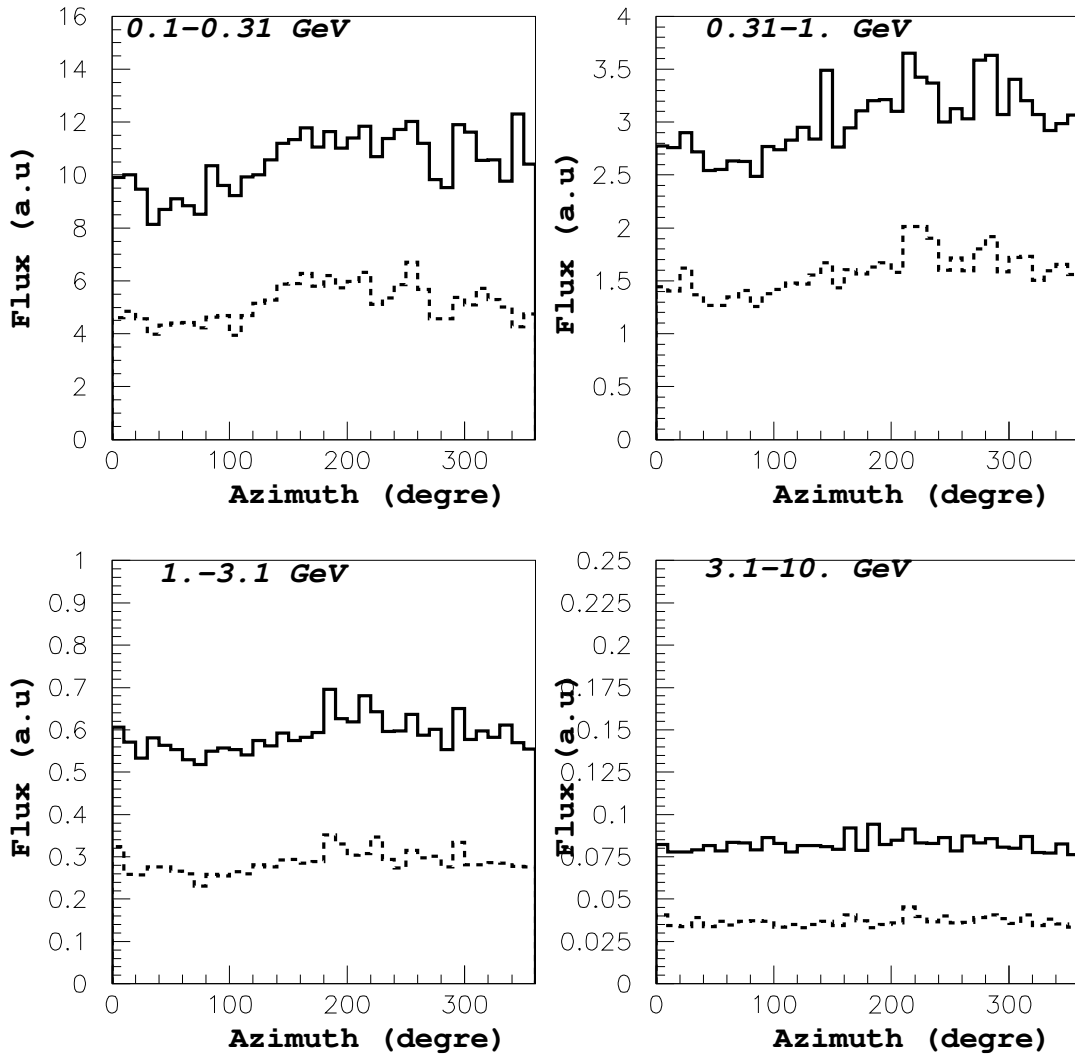


Figure 22: Same as fig.20 in the region of geomagnetical latitude  $0.6 \text{ rad} \leq |\Theta_M| \leq 1. \text{ rad}$ .

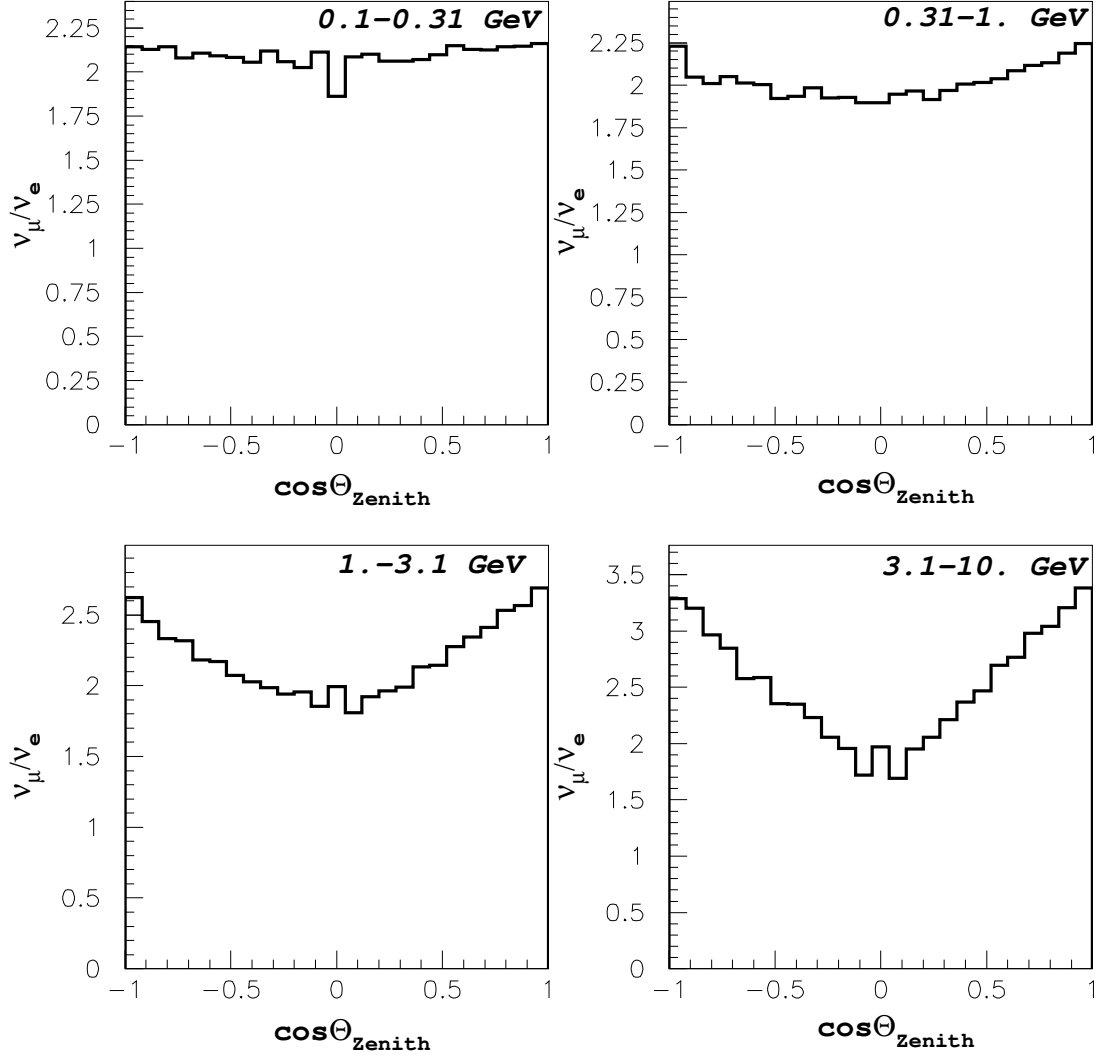


Figure 23: In the region of geomagnetical latitude  $|\Theta_M| \leq 0.2$  rad, ratio of  $(\nu_{\mu} + \bar{\nu}_{\mu})$  flux over  $(\nu_e + \bar{\nu}_e)$  flux distributions for 4 different neutrino momentum slices.



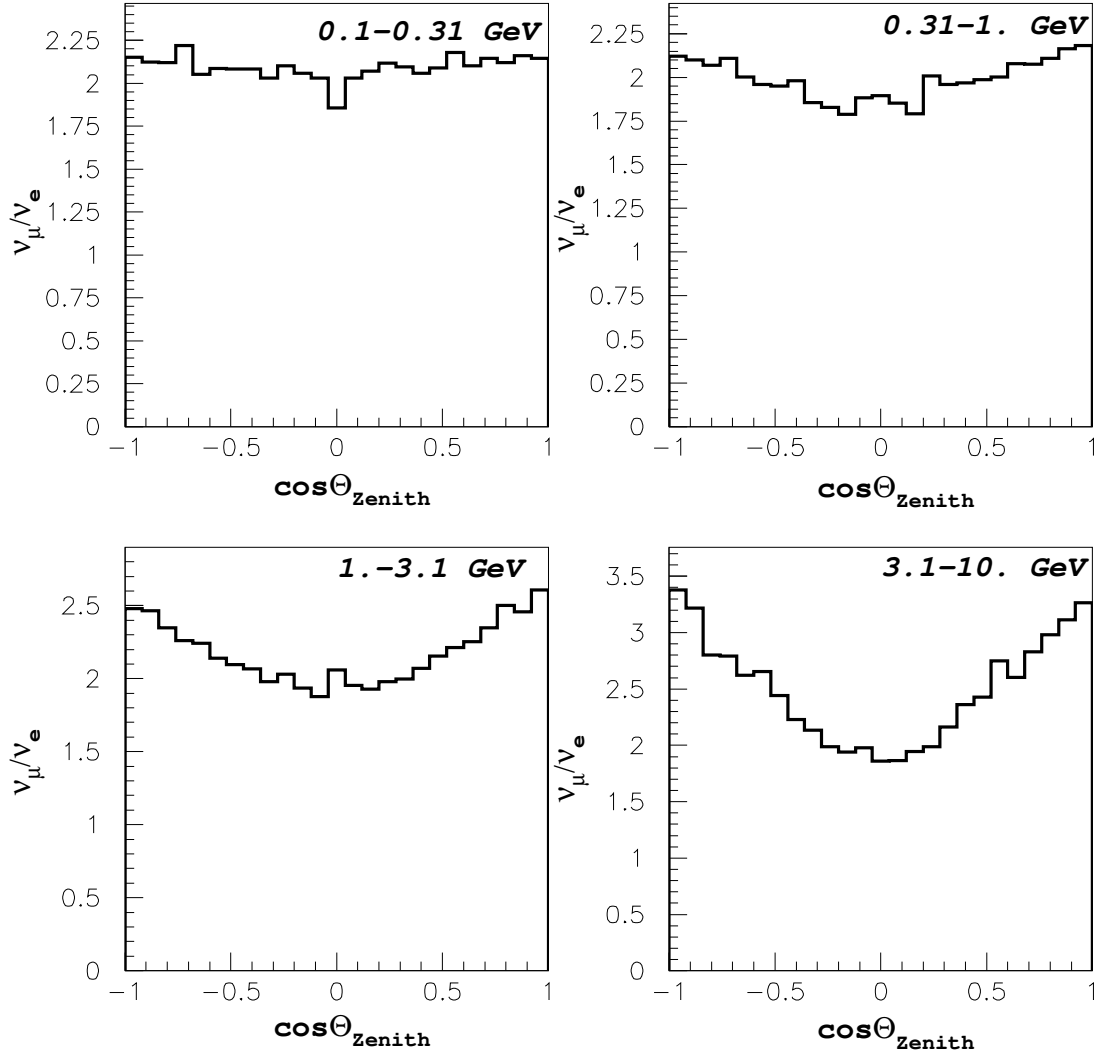


Figure 24: Same as fig.23 in the region of geomagnetical latitude  $0.2 \text{ rad} \leq |\Theta_M| \leq 0.6 \text{ rad}$ .

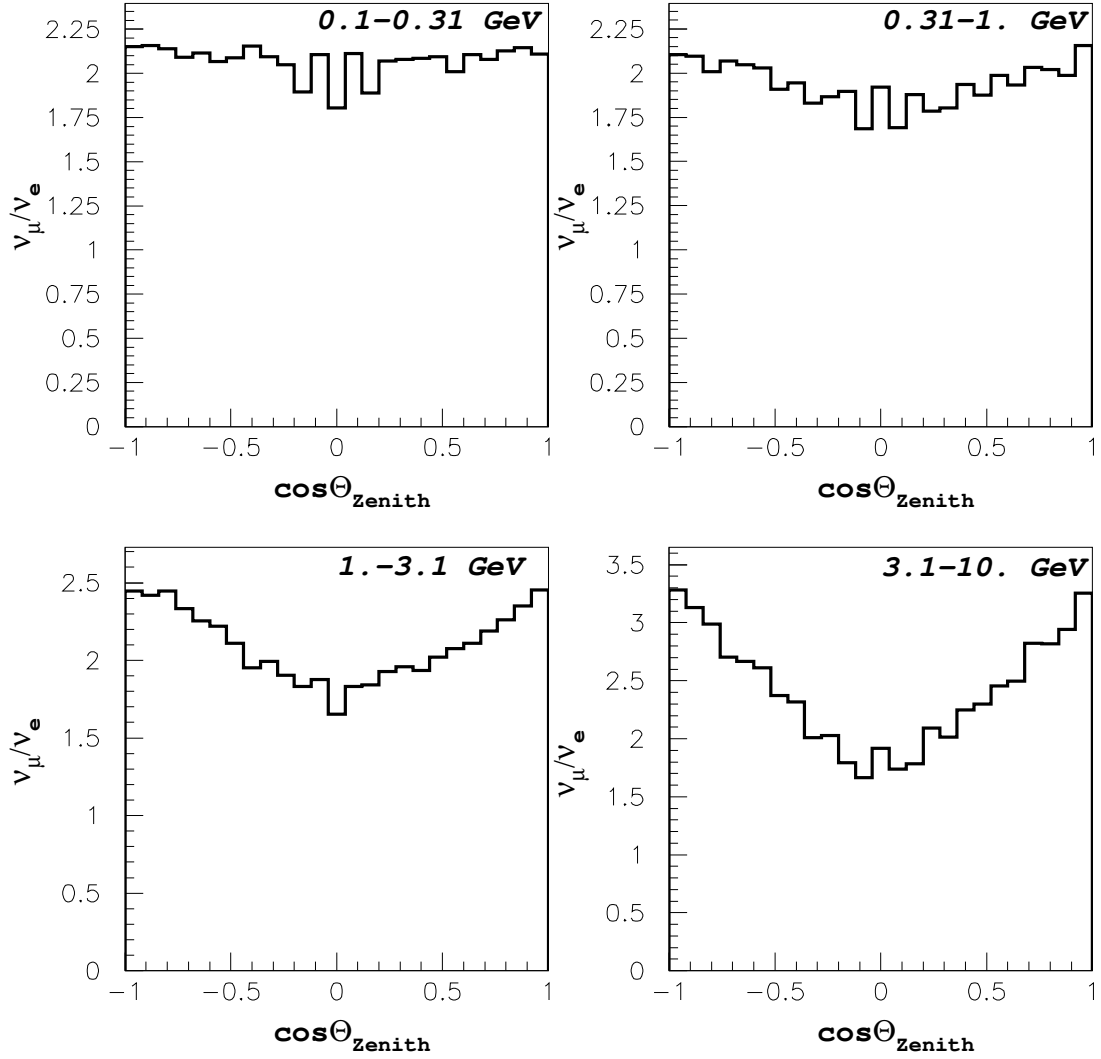


Figure 25: Same as fig.23 in the region of geomagnetical latitude  $0.6 \text{ rad} \leq |\Theta_M| \leq 1. \text{ rad}$ .

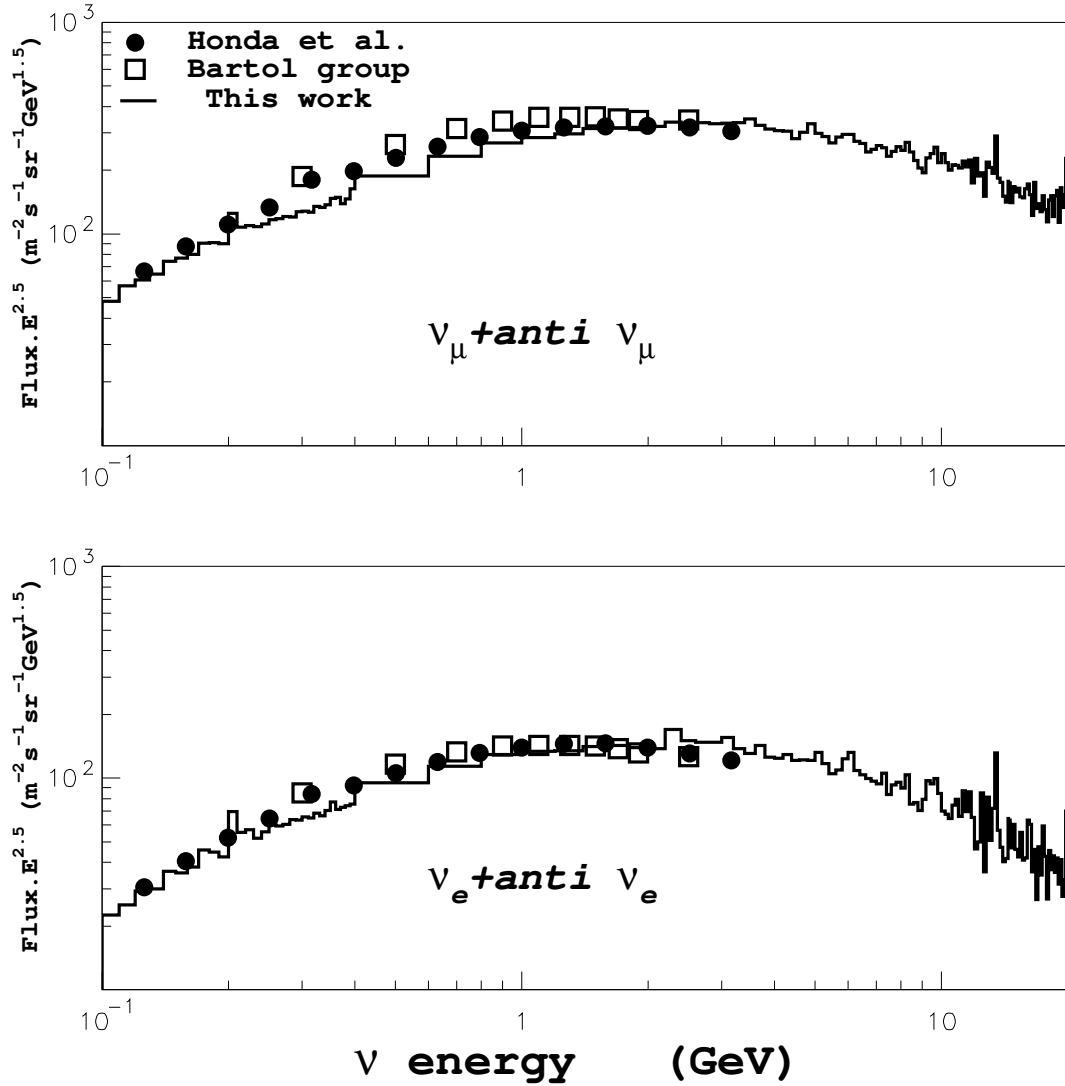


Figure 26: Flux  $\times E_\nu^{2.5}$  and averaged on angles as a function of neutrino energy. On purpose of comparison, we used here the same primary spectra as Honda et al.[1]; black dots are M.C from ref.[1], squares from ref.[2] at solar maximum.

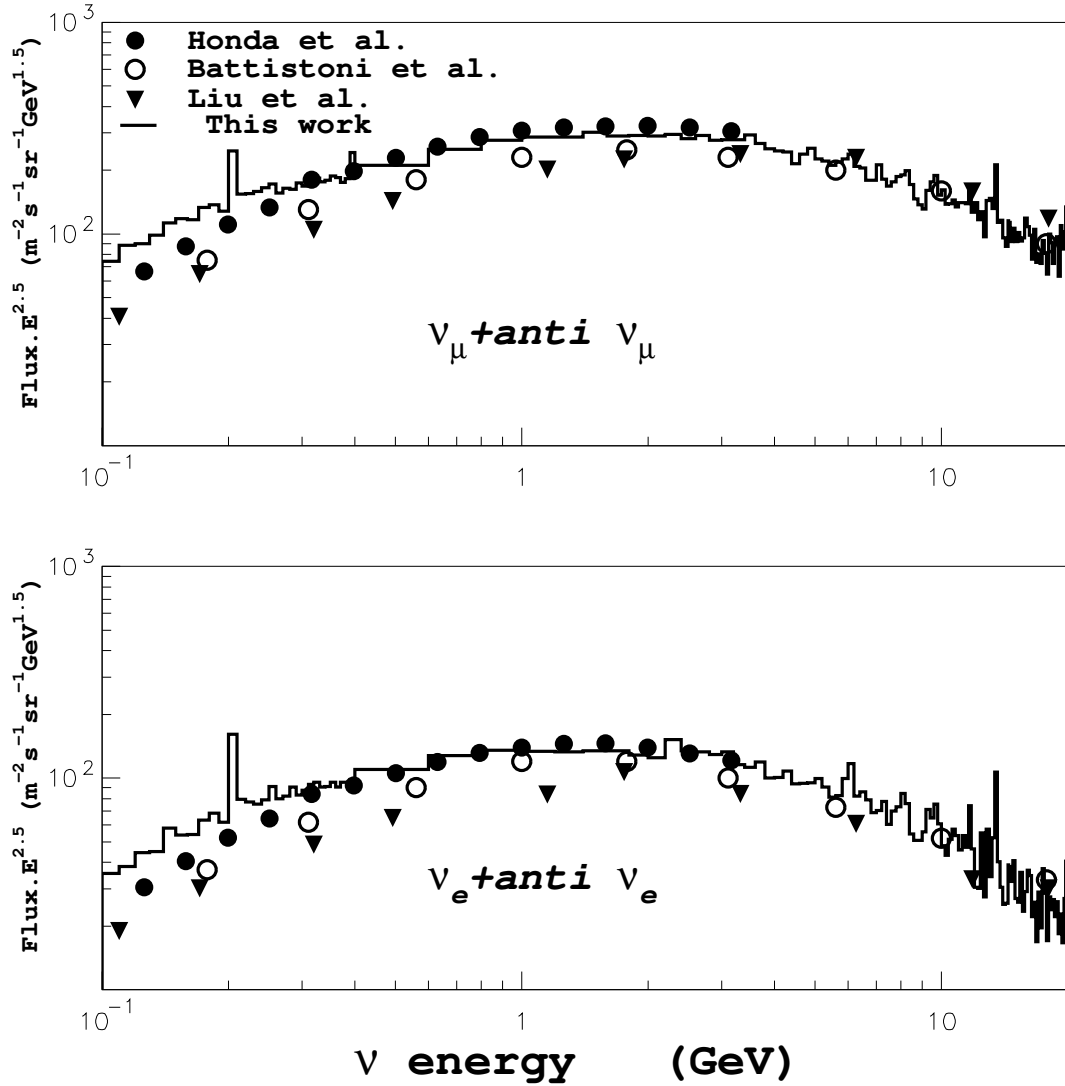


Figure 27: Flux  $\times E_{\nu}^{2.5}$  and averaged on angles as a function of neutrino energy. Here we used our AMS primary spectrum, corrected for solar modulation corresponding to years 1996,1997,1998; black dots are M.C from ref.[1], circles from ref.[4] (solar maximum), triangles from ref.[23].

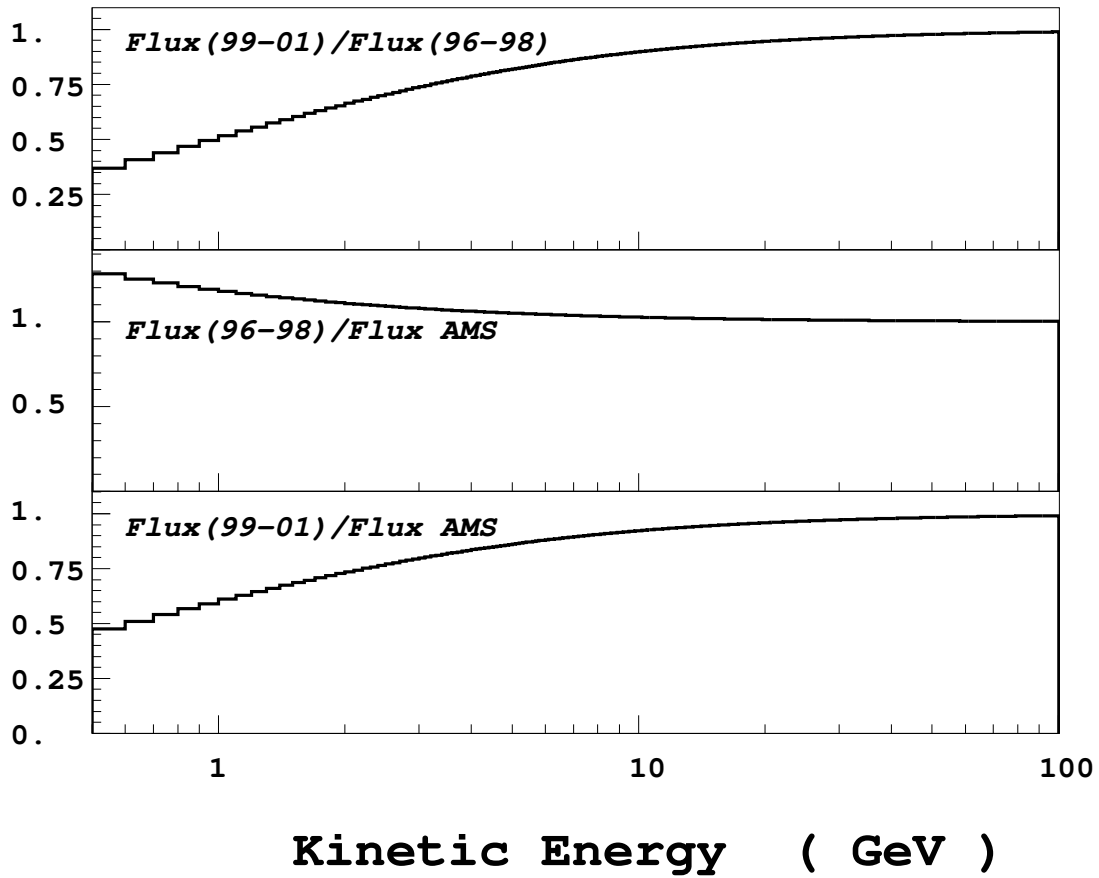


Figure 28: Ratio of primary protons spectra for three different solar activities periods: SK1=1996+1997+1998 ; SK2=1999+2000+2001; AMS: June 1998. Computed from ref.[1] formulae and CLIMAX neutron monitor data [22].

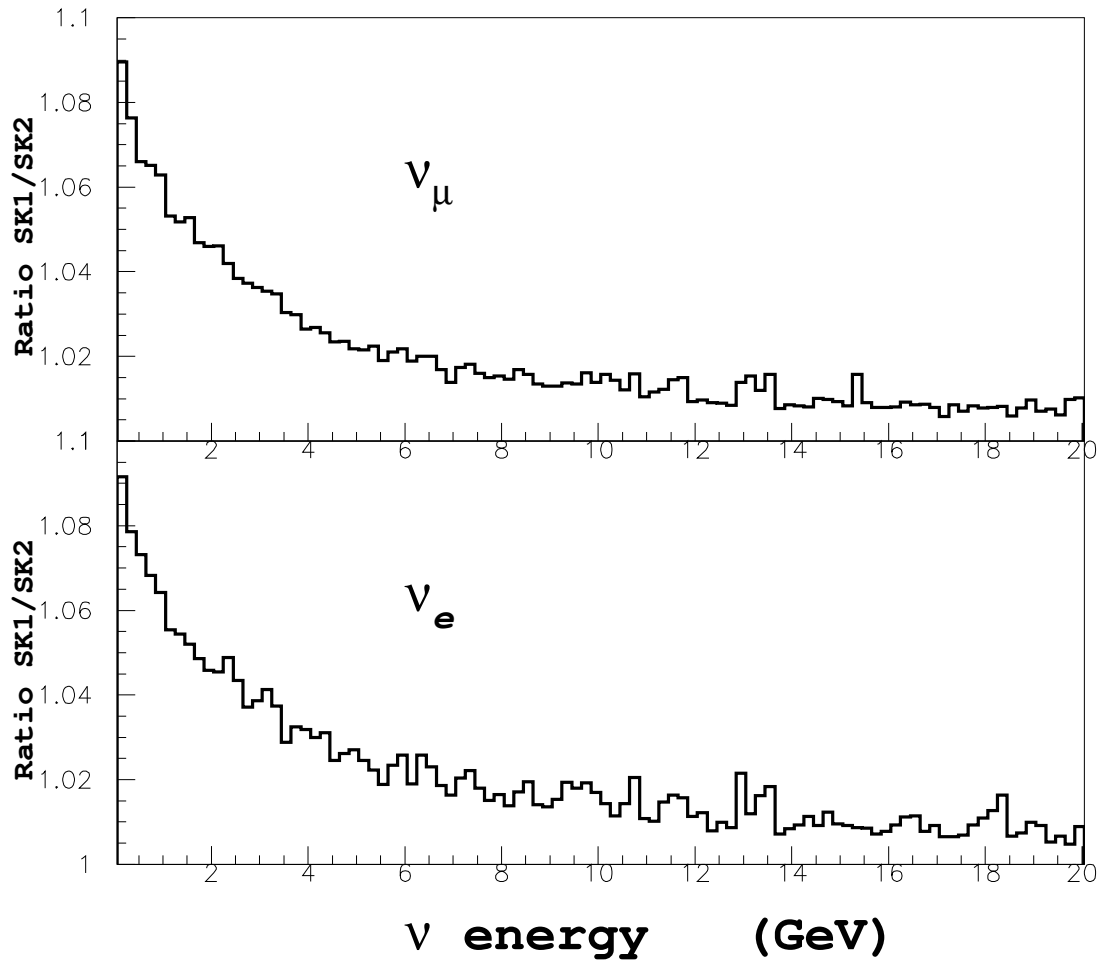


Figure 29: Ratio of neutrino spectra between SK1 (years 1996,1997,1998) and SK2 (years 1999,2000,2001), using the modulation formula of ref.[1].

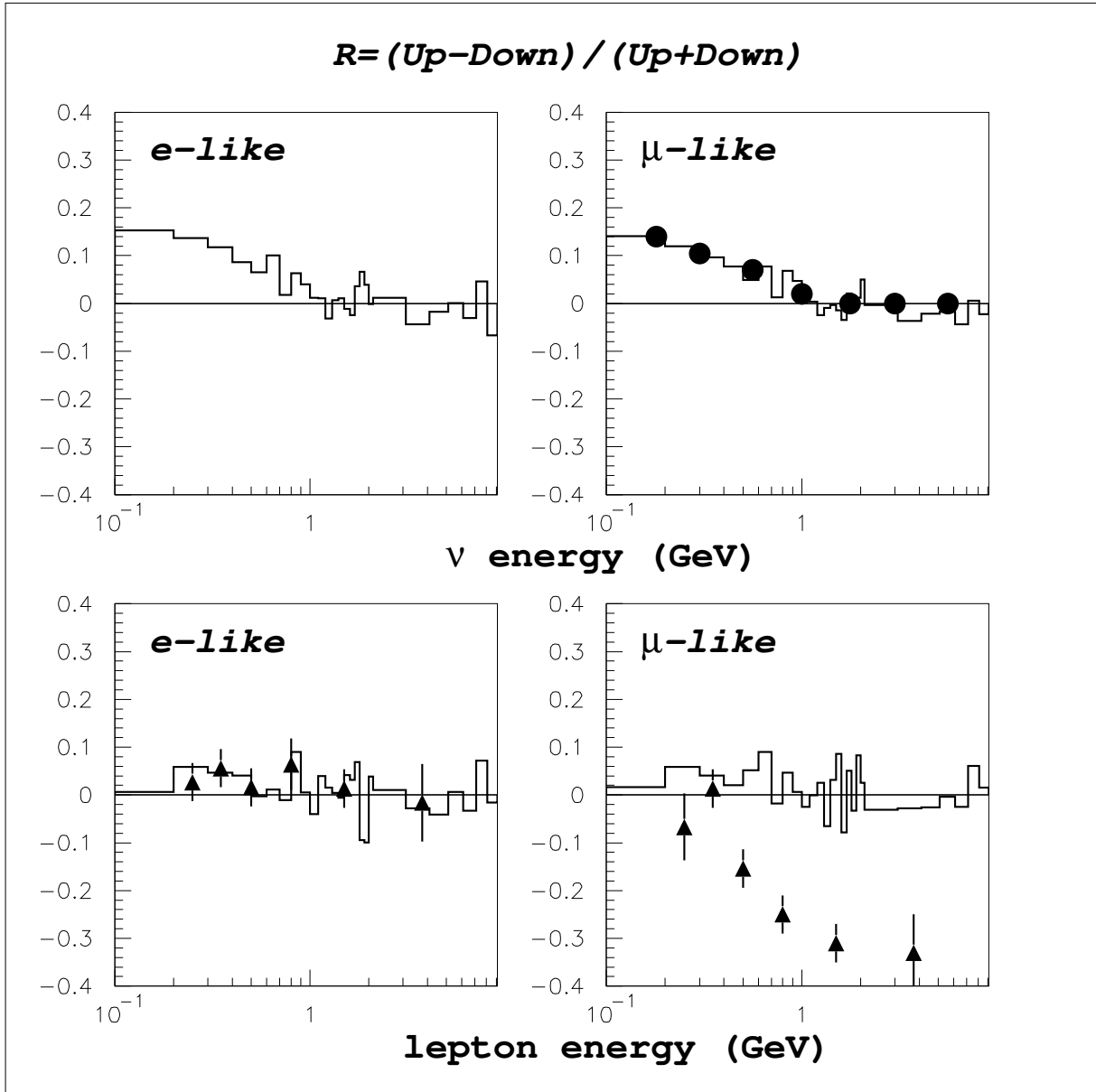


Figure 30: The up-down asymmetry is defined as the difference of up and down neutrino fluxes divided by their sum. The two top histograms use the neutrinos angles and momentum; the bottom ones use smeared induced leptons corresponding variables. The black dots are the result from a 3-D Fluka recent version M.C. (ref.[5]), and triangles are Super Kamiokande points from ref.[25]

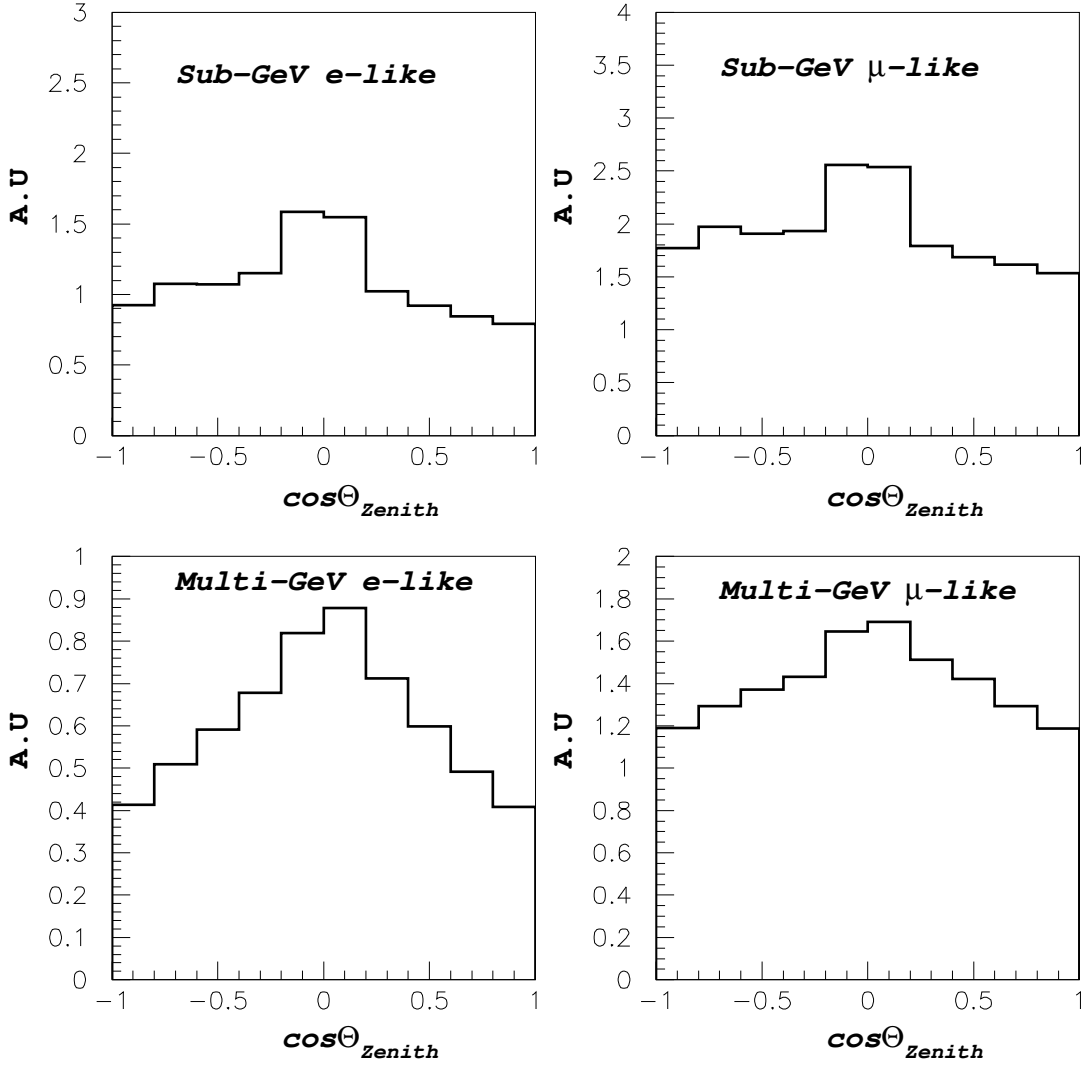


Figure 31: Variation with the zenith angle of neutrinos fluxes at Super-Kamiokande latitude. Here, no smearing is applied to the neutrinos angles and momentum.



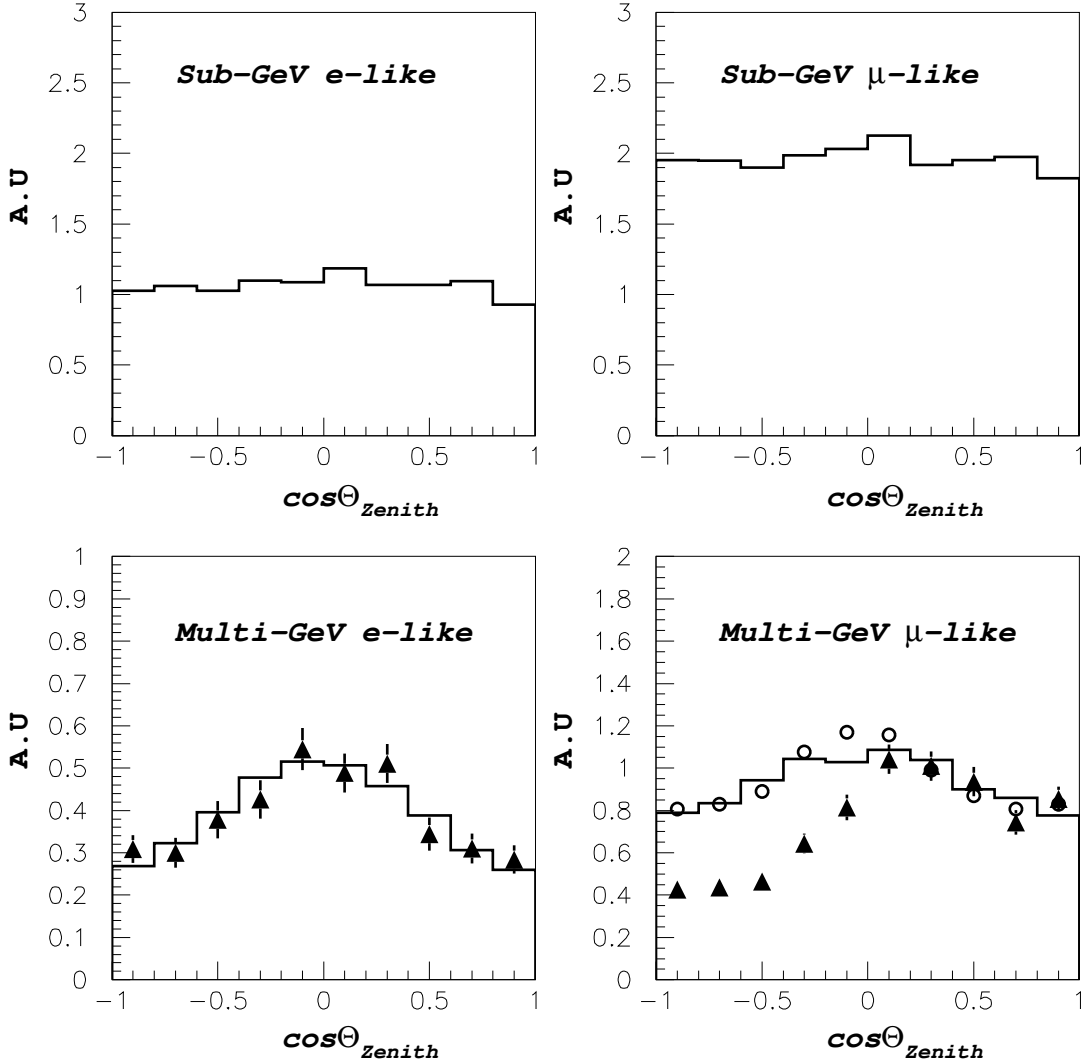


Figure 32: Variation with the zenith angle of neutrinos fluxes at Super-Kamiokande latitude. Smearing is applied to the neutrinos angles and momentum to reproduce the incertitude on the neutrino variables when the induced lepton is used. We have reproduced for the multi-GeV views the results of S.K [30](black triangles), where we normalized at equal surface for the e-like histogram, and only at the three last bins in  $\cos\theta$  for the  $\mu$  - like plot. Open circles are the Honda's M.C. results shown in[30].

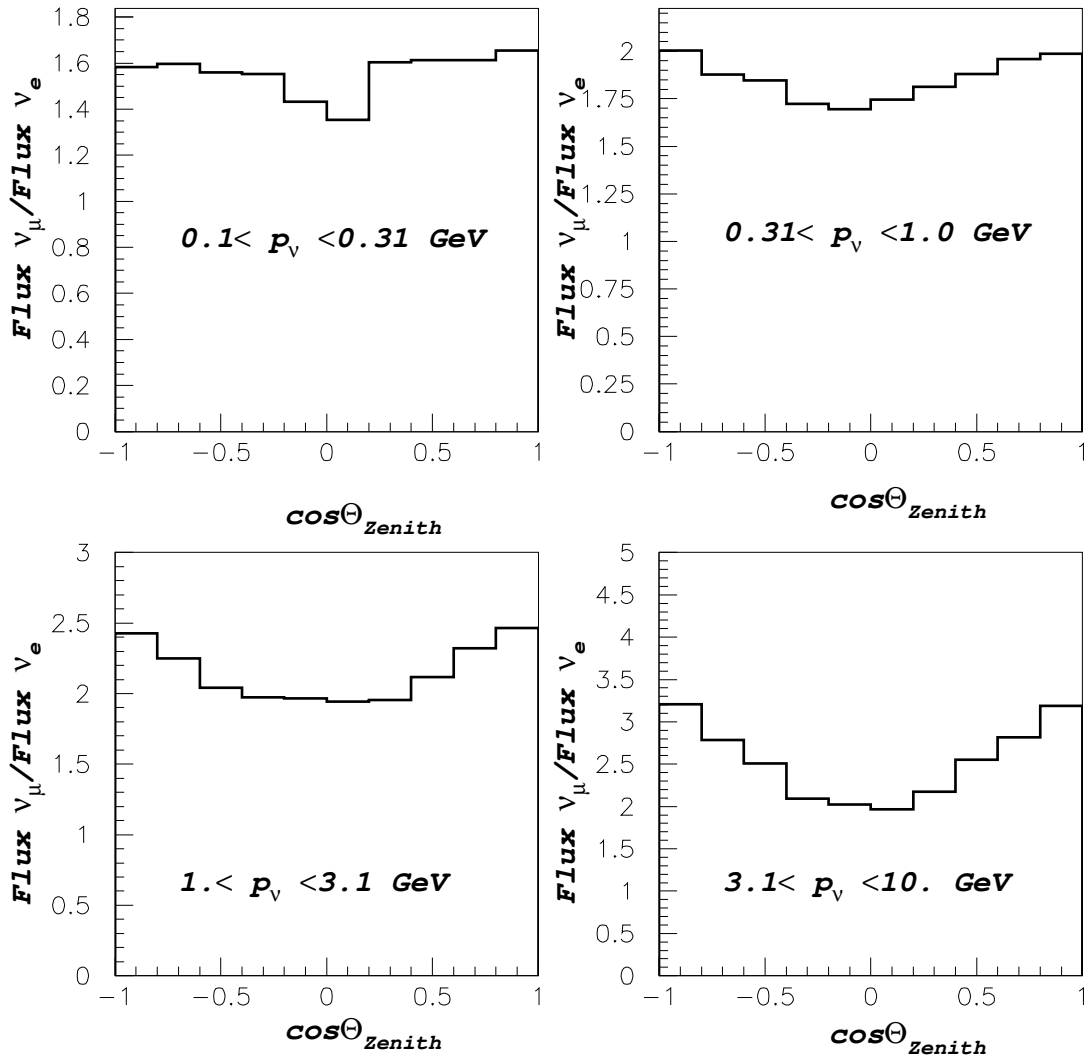


Figure 33: The ratio of fluxes  $(\nu_{\mu} + \bar{\nu}_{\mu}) / (\nu_e + \bar{\nu}_e)$  for 4 different neutrino momentum slices, at the Super-Kamiokande latitude, as a function of the zenith angle.

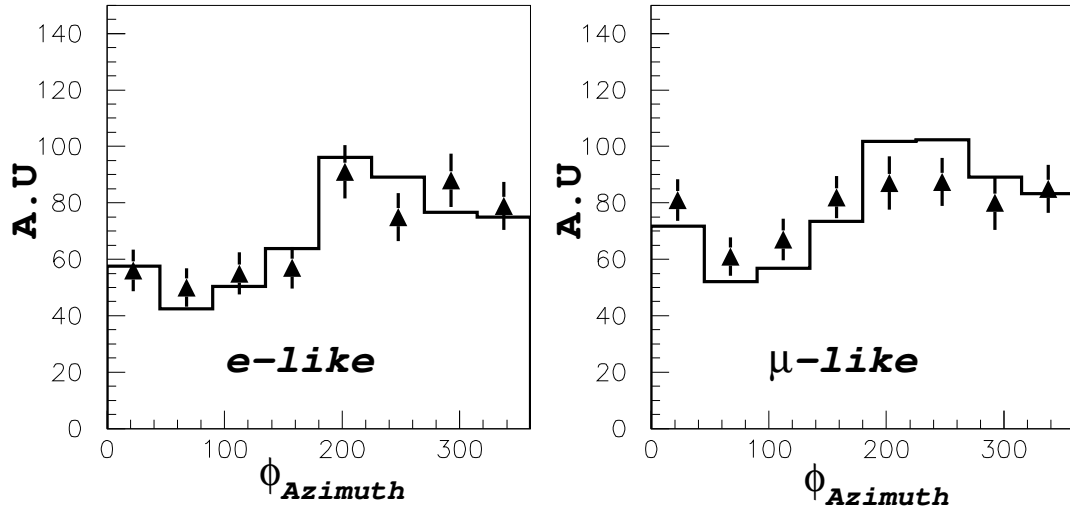


Figure 34: Comparison of Super-Kamiokande ( black triangles) and M.C for azimuthal direction of the incoming neutrino; M.C is smeared with S.K angular resolution and weighted proportionnal to neutrino cross-section; normalisation is done to the total number of S.K events. Events selection is:  $\leq 0.4 \text{ p} \leq 3. \text{ GeV}$ , and  $\text{abs}(\cos \theta_{\text{Zenith}}) \geq 0.5$  ) No oscillation is present in MC.